Unified Performance Analysis of Antenna Selection Schemes for Cooperative MIMO-NOMA With Practical Impairments

Mahmoud Aldababsa, Eray Güven, M. Akif Durmaz, Caner Göztepe, Güneş Karabulut Kurt, *Senior Member, IEEE*, and Oğuz Kucur

***Abstract*— This paper presents a unified outage probability (OP) performance analysis of two hybrid antenna selection (AS) schemes, transmit antenna selection (TAS) and maximal ratio combining (MRC), and joint transmit and receive antenna selection (JTRAS) in multiple-input multiple-output non-orthogonal multiple access based downlink amplify-and-forward (AF) relaying network with channel estimation error (CEE) and feedback delay (FD). Since the communications in the first and second hops are kinds of single-user and multi-user communications, respectively the AS is done as optimal TAS/MRC or JTRAS is applied in the first hop while the suboptimal majority-based TAS/MRC or JTRAS is employed in the second hop. For both TAS/MRC and JTRAS schemes, the OP expressions are derived in single closed-form over Nakagami-*m* fading channels in the practical and ideal cases. Moreover, in the practical case, the lower bound OP expressions are found and at high signal-to-noise ratio (SNR) values, the OP reaches an error floor value, which means zero-diversity order. In the ideal case, asymptotic OP expressions are obtained in high SNR regime and demonstrate achievable non-zero diversity and array gains. Finally, through simulations and software-defined radio-based real-time tests, the accuracy of theoretical analysis is validated.**

***Index Terms*— Outage probability, transmit antenna selection, maximal ratio combining, joint transmit and receive antenna selection, multiple-input multiple-output, non-orthogonal multiple access, channel estimation error, feedback delay, software-defined radio-based real-time tests.**

Manuscript received December 19, 2020; revised June 6, 2021 and September 28, 2021; accepted November 7, 2021. Date of publication November 30, 2021; date of current version June 10, 2022. This work was supported by the Scientific and Technological Research Council of Turkey (TÜBİTAK) under Project EEEAG-118E274. The associate editor coordinating the review of this article and approving it for publication was X. Cheng. *(Corresponding author: Mahmoud Aldababsa.)*

Mahmoud Aldababsa is with the Department of Electrical and Electronics Engineering, Istanbul Gelisim University, 34310 Istanbul, Turkey (e-mail: mhkaldababsa@gelisim.edu.tr).

Eray Güven and Caner Göztepe are with the Department of Electronics and Communication Engineering, Istanbul Technical University, 34469 Istanbul, Turkey (e-mail: guvenera@itu.edu.tr; goztepe@itu.edu.tr).

M. Akif Durmaz was with the Department of Electronics and Communications Engineering, Istanbul Technical University, 34469 Istanbul, Turkey. He is now with the Turkcell Technology 5G Research and Development Team, 34854 Istanbul, Turkey (e-mail: makif.durmaz@gmail.com).

Güneş Karabulut Kurt was with the Department of Electronics and Communications Engineering, Istanbul Technical University, 34469 Istanbul, Turkey. She is now with the Poly-Grames Research Center, Department of Electrical Engineering, Polytechnique Montréal, Montréal, QC H3T 1J4, Canada (e-mail: gunes.kurt@polymtl.ca).

Oğuz Kucur is with the Department of Electronics Engineering, Gebze Technical University, 41400 Gebze/Kocaeli, Turkey (e-mail: okucur@gtu.edu.tr).

Color versions of one or more figures in this article are available at https://doi.org/10.1109/TWC.2021.3129307.

Digital Object Identifier 10.1109/TWC.2021.3129307

I. Introduction

INCREASING demands of high spectral efficiency, high connectivity, and low latency in the fifth-generation (5G) and future generations make the researchers try to find alternative radio access technique to the current orthogonal multiple access (OMA) techniques that have the inability to cope with these challenging demands. Non-orthogonal multiple access (NOMA) has recently been considered as a promising radio access technique to satisfy the aforementioned demands [1]. Unlike the conventional OMA, the key idea in NOMA is to allocate non-orthogonal resources to serve multiple users, yielding a high spectral efficiency while allowing some degree of interference at receivers [2]. In power-domain NOMA, multiple users are superposed by different power levels opposite to their channel conditions such that successive interference cancellation (SIC) is applied at receivers, offering a good tradeoff between system throughput and user fairness [3].

In wireless communication systems, multiple-input multiple-output (MIMO) techniques play a significant role in mitigating the detrimental effects of unavoidable fading by using multiple transmitting and receiving antennas [4]. Although using multiple transmit and/or receive antennas increases the capacity and system performance, they may suffer from extra power consumption and hardware complexity caused by containing of multiple radio frequency (RF) chains. Nevertheless, antenna selection (AS) schemes are proposed as an effective solution eliminating the aforementioned drawbacks by reducing the number of RF chains and keeping the benefits of MIMO systems [5]. As well, relay assisted cooperative communications provide reliable communications at even severe fading conditions and and extend the coverage area of the systems [6]. Accordingly, both multi-antenna and cooperative techniques are for current systems and future generations. Since NOMA is a vigorous candidate to be standard for the 5G and beyond, the inclusion of MIMO and cooperative communication techniques in the NOMA is necessary to improve metrics such as outage probability (OP) and ergodic sum-rate.

A. Literature Review

Recently, various works have studied the diversity techniques in the MIMO-NOMA with or without relaying networks. For that in the MIMO-NOMA networks [2], [7]–[22], particularly, [2] examines OP and

ergodic sum-rate performance for the NOMA network with the receive diversity technique, maximal ratio combining (MRC). In addition, [7], [8]–[10], [11] and [12]–[16] study the NOMA network's performance with the transmit diversity techniques such as maximum ratio transmission (MRT), Alamouti space-time block coding (STBC), orthogonal STBC, transmit antenna selection (TAS), respectively. The selection criteria of the TAS scheme in [12]–[16] are different. For instance, in [12], the ergodic performance is investigated for the NOMA network with the TAS, offering the highest sum-rate. However, in [13], the sum-rate of the NOMA network is optimized with the TAS by considering the fairness between the mobile users. On the other hand, in [14]–[16], the NOMA networks' performance is examined with TAS taking into account the security between mobile users. So far, the OP or sum-rate or bit error rate performance is analyzed for the NOMA network with the suboptimal hybrid AS schemes such as majority-based TAS (TAS-maj)/MRC (TAS-maj)/MRC and majority-based joint transmit and receive antenna selection (JTRAS-maj) in [17]–[19] and joint AS, max-max-max (A^3) and max-min-max (AIA) in [20]–[22].

On the other hand, there are also many works using the diversity techniques in the cooperative MIMO-NOMA networks [23]–[30]. In particular, the OP and ergodic sum-rate are studied in [23] under Rayleigh fading channels for the dual-hop NOMA network, where the JTRAS scheme is applied in the 1st hop and receive antenna selection (RAS) is employed in the 2nd hop. In [24], the exact OP and its lower bound expressions are obtained for another NOMA network with multi-antenna in Rayleigh fading channels. In this network, through a channel state information (CSI) based gain amplify-and-forward (AF) relay with a single antenna, a base station (BS) communicates with multiple mobile users. The BS and mobile users are equipped with multi-antenna, and the TAS and MRC are employed at the BS and each mobile user, respectively. The OP performance of the same network in [24] is investigated in [25] for the fixed-gain AF relay. Besides, the OP performance of the network in [24] is examined in [26] and [27] for energy harvesting AF and decode-and-forward (DF) relays, respectively. The exact OP expression of the same network in [24] is also derived in [28] for the CSI based gain AF relay with presence of channel estimation error (CEE). A unified analysis of the OP performance of the same network in [24] is carried out in [29] for both CSI based and fixed-gain AF relay in the presence of CEE and SIC error. In addition, the lower and upper bounds of the ergodic sum-rate are obtained. The OP performance is investigated in [30] for dual-hop NOMA network with CSI based AF relay, in which the MRT/RAS technique is applied in both hops with CEE.

B. Motivations and Contributions

Based on the related works presented above, we have some notices highlighted as follows: (1) The works [23]–[27] assume no practical impairment conditions. But this assumption is too optimistic and does not not reflect the real impairments in practice. In addition, [23]–[24] analyze the networks over Rayleigh Nevertheless, the Nakagami-*m* fading model fits very well with the empirical data better than the Rayleigh fading model and is capable of modeling a wide class of fading channel conditions, which comprises the Rayleigh fading model, i.e., $m = 1$ as a special case. (2) The reference [23] uses relay with single-transmit and multi-receive antennas while [24]–[29] use relay with single-transmit/receive antenna. However, relay with multi-transmit/receive antenna provides better system performance than that of relay with single or multi-receive antenna. (3) In spite of the benefits of AS schemes mentioned before, we notice that there is no attempt to exploit the advantages of employing AS schemes TAS and JTRAS in the 2nd hop of the dual-hop NOMA networks. This can be interpreted as that the optimal AS is not possibly achieved in multi-user networks such as NOMA. Different from the conventional OMA, the AS schemes have to be wholly carried out in the NOMA network regarding whole users to find the best transmit antenna, however, finding the same best transmit antenna of the relay for whole users may not be possible for all channel realizations. In addition, the signals in the conventional OMA are conveyed in an interference-free manner, however, in the NOMA, there are severe inter-user interferences. Therefore, because of interference according to reception using the SIC and power domain transmission, the AS based NOMA networks' mathematical analyses are more difficult. Because of that, there are some attempts to apply suboptimal AS solutions such as A^3 and AIA [20]–[22], and TAS-maj and JTRAS-maj [17]–[19]. However, some results in [17]–[19] show the superiority of the AS schemes that based on majority over the AS schemes that based on A^3 and AIA. Such A^3 and AIA based AS schemes aim to enhance the near user's and far user's performance, respectively while majority-based AS schemes aim to improve more than half of users' performance. (4) The studies [28]–[30] consider only CEE and/or imperfect SIC and neglect the effect of the feedback delay (FD). However, the FD is also a real strong problem the NOMA networks face.

To the best of our knowledge and with the above motivations, for the first time in the literature we study the OP of dual-hop MIMO-NOMA network in the practical (CEE&FD) and ideal cases. In the network, the BS, CSI based gain AF relay and mobile users are equipped with multiple antennas and two different AS schemes (TAS/MRC and JTRAS) are applied symmetrically in both hops. Note that the AS is done as follows: In the 1st hop, the optimal AS (TAS/MRC or JTRAS) [31] scheme is employed since the communication in the 1st hop is a kind of single-user communication. On the other hand, in the 2nd hop, the corresponding majority-based AS (TAS-maj/MRC or JTRAS-maj) scheme [17]–[19], developed for NOMA, is employed since the communication in the 2nd hop is multi-user communication. The main contributions of the paper can be summarized as follows: (1) The unified analysis of the two AS schemes, TAS/MRC and JTRAS, for the OP performance of the cooperative MIMO-NOMA network is provided in the ideal and practical conditions. (2) For TAS/MRC and JTRAS schemes, the single closed-form of the exact OP expressions is derived for all mobile users

over Nakagami-m fading channels. (3) To provide insight into OP behavior in the practical conditions, the lower bound OP expression is obtained. It is observed that in the high signal-to-noise ratio (SNR) region, the OP does not depend on SNR values and reveals a fixed value, error floor (EF) value, which eliminates the system's diversity gain. (4) The high SNR analysis is carried out in the ideal condition to obtain asymptotic OP expression. It is noticed that the OP is still proportionate to SNR values, which means that the system achieves both diversity and array gains. (5) Software-defined radio (SDR) implementations of both schemes, which are the most elaborated NOMA implementations in the literature, are realized. (6) The analytical results are verified by the Monte-Carlo simulations and SDR-based real-time tests, and a comprehensive comparison between the AS schemes, TAS/MRC and JTRAS performances is performed as well as the suboptimal majority-based AS schemes are compared to the previous suboptimal A^3 and AIA based AS schemes. Also, shown that the OP performance of all users converges to the same value as CEE and/or FD rises. In addition, for all users the optimal relay location becomes closer to the middle in the practical case unlike that in the ideal case. Besides, the effect of antenna configuration of hopes is different on the users.

The organization of paper is given as following: In Section II, the models of the system and channel are described. The performance analysis is conducted in Section III. In Section IV, the designed test-bed for SDR-based real time tests of the systems is explained. In Section V, the numerical results are demonstrated and in Section VI, the paper concluded. Throughout this paper, $P_r(\cdot)$ symbolizes probability; $F_X(x)$ and $f_X(x)$ denote cumulative distribution function (CDF) and probability density function (PDF) of a random variable X, respectively; $|\cdot|$, $E[\cdot]$, $(\cdot)^H$ and $\boldsymbol{I}_N$ represent the absolute value, expectation operator, Hermitian transpose and identity matrix of order N, respectively; $\Psi(\cdot,\cdot)$ and $\Gamma(\cdot)$ are lower incomplete Gamma function and Gamma function, respectively; $\|\cdot\|$ denotes Frobenius norm and $K_u(\cdot)$ denotes the uth order of modified Bessel function of the second kind.

II. System and Channel Models

As shown in Fig. 1, we consider downlink relaying assisted MIMO-NOMA networks. The BS communicates with multiple mobile users (L) simultaneously with the help of a CSI based gain AF relay. All nodes have multi-antenna, the BS and mobile users typically are equipped with N_{t_1} transmit and N_{r_2} receive antennas, respectively as well as the relay is equipped with N_{r_1} receive and N_{t_2} transmit antennas. Since the BS and mobile users are located far away from each other or within heavily shadowed areas, the direct links between them are unavailable. All mobile users are clustered very close such that homogeneous network topology is considered. It is assumed that the fading channel coefficients of the 1st hop between the BS's ith antenna and the relay's jth receive antenna are $h_1^{(i,j)}$, where $i = 1,\ldots,N_{t_1}$, $j = 1,\ldots,N_{r_1}$ and $\Omega_1 = E[|h_1^{(i,j)}|^2]$. Also, the fading channel coefficients of the 2nd hop between the relay's ith antenna and the lth user (U_l)'s jth receive antenna is $h_{2,l}^{(i,j)}$, where $i = 1,\ldots,N_{t_2}$, $j = 1,\ldots,N_{r_2}$, $l = 1,\ldots,L$ and $\Omega_2 = E[|h_{2,l}^{(i,j)}|^2]$. Let d_1 and d_2 denote the distances between the BS and relay, the relay and mobile users, respectively. Then, $\Omega_1 = {d_1}^{-\alpha}$ and $\Omega_2 = {d_2}^{-\alpha}$, where α denotes path loss exponent. In this paper, two different AS schemes are applied in both hops: TAS/MRC as in Fig. 1a and JTRAS as in Fig. 1b. In this section, at first the majority-based TAS/MRC and JTRAS schemes are clearly explained. Then, the system models for cooperative MIMO-NOMA network with (TAS/MRC or JTRAS) scheme are described.

TABLE I

TAS-maj/MRC and JTRAS-maj Schemes

Scheme	TAS-maj/MRC	JTRAS-maj
Selection Criterion	• Apply the optimal TAS/MRC separately for each user. • Find the index of the best transmit antenna which provides the maximum sum of squared channel gains between the relay and users. Let's label this index with i_l^{opt} for lth user. • Apply the majority rule to the set of i_l^{opt} to find the index of the majority transmit antenna i^{maj}	• Apply the optimal JTRAS separately for each user. • Find the indices of the best transmit-receive antenna pair which provides the maximum squared channel gains between the relay and users. Let's label these indices with (i_l^{opt}, j_l^{opt}) for lth user. • Apply the majority rule to the set of i_l^{opt} to find the index of the majority transmit antenna i^{maj}

Example

i_1^{opt}	i_2^{opt}	i_3^{opt}	i^{maj}
1	1	1	1
1	1	2	1
1	2	1	1
2	1	1	1
1	2	2	2
2	1	2	2
2	2	1	2
2	2	2	2

A. Preliminary to TAS-maj/MRC and JTRAS-Maj Schemes

The majority-based AS schemes basically depend on the majority rule to determine the majority transmit antenna. They have been suggested in the multi-user NOMA networks (as in the second hop) as alternative suboptimal AS solutions to the optimal AS schemes, which are achieved in the single-user communication network (as in the first hop) but not possibly achieved in the multi-user NOMA networks. In this paper, we will use two majority-based schemes; TAS-maj/MRC and JTRAS-maj. The selection criterion for each scheme is explained in detail in Table I. Then, we give an example to understand the concept well. With respect to Figures 1a-1b, assume that there are three users equipped with two receive antennas and the relay equipped with two transmit antennas. Accordingly, the probable optimal transmit antenna at the relay for each user (i_l^{opt}) is specified in Table I. Next, the possible majority transmit antenna (i^{maj}) is determined. Note that $i_l^{opt} = 1$ means that the first transmit antenna at the relay is selected when the optimal TAS/MRC or JTRAS scheme is applied between the relay and lth user, whereas $i_l^{opt} = 2$ means that the second transmit antenna at the relay is selected when the optimal TAS/MRC or JTRAS scheme is applied between the relay and lth user. On the other hand, $i^{maj} = 1$ means that the majority selected transmit antenna belonging to the set $\{i_1^{opt}, i_2^{opt}, i_3^{opt}\}$ is the first transmit antenna, while $i^{maj} = 2$ means that the majority selected transmit antenna belonging to the set $\{i_1^{opt}, i_2^{opt}, i_3^{opt}\}$ is the second transmit antenna.

B. Cooperative MIMO-NOMA Network's System Model With TAS/MRC Scheme

As shown in Fig. 1a, the AS is done as follows: In the 1st hop, the optimal TAS/MRC [31] scheme is employed. Such a transmit antenna at the BS, i_1, is selected, which has the maximum sum of the squared channel gains between receiver

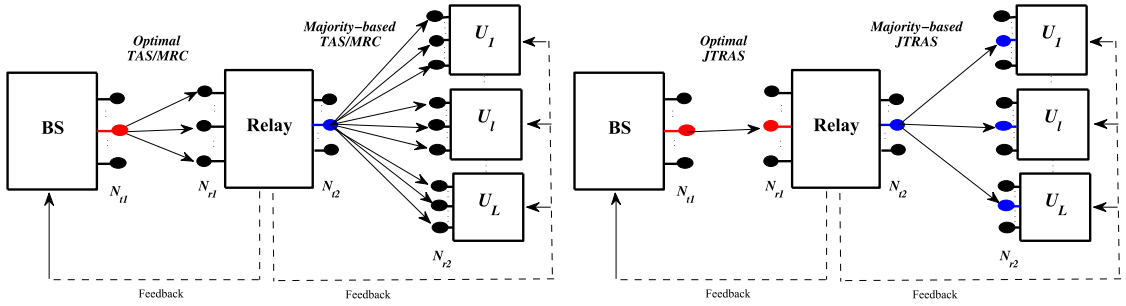

(a) TAS/MRC scheme (b) JTRAS scheme

Fig. 1. The cooperative MIMO-NOMA network's system model with different AS schemes.

antennas of the relay. On the other hand, in the 2nd hop, the TAS-maj/MRC scheme [17], [18], is employed. Thus, the transmit antenna at the relay, i_2, is selected, which has the maximum total of squared channel gains for more than half of the users. We assume that the BS has the necessary CSI's knowledge and channel quality's order for the links between the relay and users. During the training period, in the 1st hop, the BS sends pilot symbols to the relay, whereas in the 2nd hop, by assuming that uplink and downlink channels are reciprocal, each user sends pilot symbols to the relay. Next, the relay estimates the links' channel gains in both hops and then specifies and sends the index of the BS's best transmit antenna and the lookup table's row code, which represents the channel quality's order for the 2nd hop links and power coefficients to the BS, and the estimated coefficients of the 2nd hop links to the users through feedback channels. Note that this type of training is assumed for the fixed relay. For the mobile relay, training in the 1st hope can be done in uplink in order to reduce the load of the relay, i.e., BS estimates channel coefficients and sends them to the relay and also determines its best transmit antenna. As explained later, any type of training will not change the model of the analysis.

The whole communication process is completed in two time slots. Assume that P_1 is the transmit power, x_i is U_i's information with unit energy, and a_i is U_i's power allocation coefficient with $\sum_{i=1}^{L} a_i = 1$. Note that $a_1 > a_2 > \ldots > a_L$ reverse to the order of 2nd hop channel gains based on NOMA concept. Then, during the 1st slot, the BS superimposes the users' signals into one signal, $x_t = \sqrt{P_1}\sum_{i=1}^{L}\sqrt{a_i}x_i$. Next, the BS transmits the signal x_t to the relay. Hence, the received signal at the relay, $\boldsymbol{y}_1$, can be expressed as

$$\boldsymbol{y}_1 = \boldsymbol{h}_1 x_t + \boldsymbol{n}_1 = \boldsymbol{h}_1\sqrt{P_1}\sum_{i=1}^{L}\sqrt{a_i}x_i + \boldsymbol{n}_1, \tag{1}$$

where $\boldsymbol{h}_1$ is the $N_{r_1} \times 1$ 1st hop's fading channel coefficient vector between the selected transmit antenna i_1 at the BS and relay, and $\boldsymbol{n}_1$ is the $N_{r_1} \times 1$ zero mean complex additive Gaussian noise with $E[\boldsymbol{n}_1\boldsymbol{n}_1^H] = \boldsymbol{I}_{N_{r_1}}\sigma_1^2$ at the relay and σ_1^2 is each element's variance in $\boldsymbol{n}_1$. According to the MRC scheme, the received signals at the relay are combined into r_1

$$r_1 = \boldsymbol{w}_1\boldsymbol{y}_1 = \boldsymbol{w}_1\boldsymbol{h}_1\sqrt{P_1}\sum_{i=1}^{L}\sqrt{a_i}x_i + \boldsymbol{w}_1\boldsymbol{n}_1, \tag{2}$$

where $\boldsymbol{w}_1$ is the optimal receive weight vector of the 1st hop expressed as $\boldsymbol{w}_1 = \frac{\boldsymbol{h}_1^H}{\|\boldsymbol{h}_1\|}$ and $\| \boldsymbol{w}_1 \| = 1$. In the 2nd slot, the combined signal at the relay is amplified by an amplifying factor, $G = \sqrt{\frac{1}{P_1\|\boldsymbol{h}_1\|+\sigma_1^2}}$. Then, the amplified signal is sent to each user. Hence, the received signal at U_l is given as

$$\begin{aligned}\boldsymbol{y}_{2,l} &= \boldsymbol{h}_{2,l}G\sqrt{P_2}r_1 + \boldsymbol{n}_{2,l}\\ &= \boldsymbol{w}_1\boldsymbol{h}_1\boldsymbol{h}_{2,l}G\sqrt{P_1P_2}\sum_{i=1}^{L}\sqrt{a_i}x_i\\ &\quad +\boldsymbol{w}_1\boldsymbol{h}_{2,l}G\sqrt{P_2}\boldsymbol{n}_1 + \boldsymbol{n}_{2,l},\end{aligned} \tag{3}$$

where $\boldsymbol{h}_{2,l}$ is the $N_{r_2} \times 1$ 2nd hop's fading channel coefficient vector between the selected majority transmit antenna i_2 at the relay and U_l, and $\boldsymbol{n}_{2,l}$ is the $N_{r_2} \times 1$ zero mean complex additive Gaussian noise with $E[\boldsymbol{n}_{2,l}\boldsymbol{n}_{2,l}^H] = \boldsymbol{I}_{N_{r_2}}\sigma_{2,l}^2$ at the U_l and $\sigma_{2,l}^2$ is each element's variance in $\boldsymbol{n}_{2,l}$. Next, the received signals are combined by the U_l according to the MRC scheme. Thus, the combined signal at U_l, $r_{2,l} = \boldsymbol{w}_{2,l}\boldsymbol{y}_{2,l}$ is stated as

$$\begin{aligned}r_{2,l} &= \boldsymbol{w}_{2,l}(\boldsymbol{w}_1\boldsymbol{h}_1\boldsymbol{h}_{2,l}G\sqrt{P_1P_2}\sum_{i=1}^{L}\sqrt{a_i}x_i\\ &\quad +\boldsymbol{w}_1\boldsymbol{h}_{2,l}G\sqrt{P_2}\boldsymbol{n}_1 + \boldsymbol{n}_{2,l})\\ &= \boldsymbol{w}_1\boldsymbol{w}_{2,l}\boldsymbol{h}_1\boldsymbol{h}_{2,l}G\sqrt{P_1P_2}\sum_{i=1}^{L}\sqrt{a_i}x_i\\ &\quad +\boldsymbol{w}_1\boldsymbol{w}_{2,l}\boldsymbol{h}_{2,l}G\sqrt{P_2}\boldsymbol{n}_1 + \boldsymbol{w}_{2,l}\boldsymbol{n}_{2,l}\\ &= \boldsymbol{w}_1\boldsymbol{w}_{2,l}\boldsymbol{h}_1\boldsymbol{h}_{2,l}G\sqrt{P_1P_2}\sqrt{a_l}x_l\\ &\quad +\boldsymbol{w}_1\boldsymbol{w}_{2,l}\boldsymbol{h}_1\boldsymbol{h}_{2,l}G\sqrt{P_1P_2}\sum_{i\neq l}^{L}\sqrt{a_i}x_i\\ &\quad +\boldsymbol{w}_1\boldsymbol{w}_{2,l}\boldsymbol{h}_{2,l}G\sqrt{P_2}\boldsymbol{n}_1 + \boldsymbol{w}_{2,l}\boldsymbol{n}_{2,l},\end{aligned} \tag{4}$$

where $\boldsymbol{w}_{2,l} = \frac{\boldsymbol{h}_{2,l}^H}{\|\boldsymbol{h}_{2,l}\|}$ is the optimal receive weight vector of the 2nd hop for U_l with $\| \boldsymbol{w}_{2,l} \| = 1$.

Real wireless communication systems may suffer from many kinds of practical impairments, for instance CEE&FD. Therefore, the channel coefficients estimated at the relay (or BS) experience CEE. In addition, for the fixed relay, in the 1st hop, we assume that the relay sends the index of the selected antenna to the BS with a delay. Also, due to the FD [32], the channel coefficients used at the relay undergo CEE&FD (Note that for the mobile relay the channel coefficients are estimated at the BS with CEE and fed back to the relay with FD. Thus, for any type of training (or relay) the model does not change in the 1st hop). On the other hand, in the 2nd hop, since the relay

estimates the 2nd hop links' coefficients with CEE and then sends them to the users through feedback channels with FD, the channel coefficients used at the users undergo CEE&FD. Besides, the CEE between the reciprocal channels is included through modeling. Now, to model the system in the practical case, firstly, let's define some notations:

- $\hat{\boldsymbol{h}}_1$ and $\hat{\boldsymbol{h}}_{2,l}$: the $N_{r_1} \times 1$ estimated channel coefficient vector of $\boldsymbol{h}_1$ with $\hat{\Omega}_1 = E[\| \hat{\boldsymbol{h}}_1 \|^2]$ and $N_{r_2} \times 1$ estimated channel coefficient vector of $\boldsymbol{h}_{2,l}$ with $\hat{\Omega}_2 = E[\| \hat{\boldsymbol{h}}_{2,l} \|^2]$, respectively.
- $\boldsymbol{e}_{1,cee}$ and $\boldsymbol{e}_{2,l,cee}$: the $N_{r_1} \times 1$ CEE vector of the 1st hop and $N_{r_2} \times 1$ CEE vector of the 2nd hop, respectively. The $\boldsymbol{e}_{1,cee}$ and $\boldsymbol{e}_{2,l,cee}$ are statistically independent of $\hat{\boldsymbol{h}}_1$ and $\hat{\boldsymbol{h}}_{2,l}$ and modelled as complex Gaussian random variables [33] with zero mean and $E[\boldsymbol{e}_{1,cee}\boldsymbol{e}_{1,cee}^H] = \boldsymbol{I}_{N_{r_1}}\sigma^2_{e_{1,cee}}$ and $E[\boldsymbol{e}_{2,l,cee}\boldsymbol{e}_{2,l,cee}^H] = \boldsymbol{I}_{N_{r_2}}\sigma^2_{e_{2,l,cee}}$, respectively. Here, $\sigma^2_{e_{1,cee}} = \Omega_1 - \hat{\Omega}_1$ is each element's variance in $\boldsymbol{e}_{1,cee}$ and $\sigma^2_{e_{2,l,cee}} = \Omega_2 - \hat{\Omega}_2$ is each element's variance in $\boldsymbol{e}_{2,l,cee}$.
- $\hat{\boldsymbol{h}}_1^{(\tau)}$ and $\hat{\boldsymbol{h}}_{2,l}^{(\tau)}$: the $N_{r_1} \times 1$ feedback delayed version vector of the estimated channel vector $\hat{\boldsymbol{h}}_1$ and $N_{r_2} \times 1$ feedback delayed version vector of the estimated channel vector $\hat{\boldsymbol{h}}_{2,l}$, with $\hat{\Omega}_1^{(\tau)} = E[\| \hat{\boldsymbol{h}}_1^{(\tau)} \|^2]$ and $\hat{\Omega}_2^{(\tau)} = E[\| \hat{\boldsymbol{h}}_{2,l}^{(\tau)} \|^2]$, respectively. Without loss of generality, $\hat{\boldsymbol{h}}_1$ and $\hat{\boldsymbol{h}}_1^{(\tau)}$'s variances, and $\hat{\boldsymbol{h}}_{2,l}$ and $\hat{\boldsymbol{h}}_{2,l}^{(\tau)}$'s variances are assumed to be equivalent [34], i.e., $\hat{\Omega}_1 = \hat{\Omega}_1^{(\tau)}$ and $\hat{\Omega}_2 = \hat{\Omega}_2^{(\tau)}$.
- $\boldsymbol{e}_{1,fd}$ and $\boldsymbol{e}_{2,l,fd}$: the $N_{r_1} \times 1$ FD error vector of the 1st hop and $N_{r_2} \times 1$ FD error vector of the 2nd hop, respectively. The $\boldsymbol{e}_{1,fd}$ and $\boldsymbol{e}_{2,l,fd}$ are zero mean complex Gaussian random variables with $E[\boldsymbol{e}_{1,fd}\boldsymbol{e}_{1,fd}^H] = \boldsymbol{I}_{N_{r_1}}\sigma^2_{e_{1,fd}}$ and $E[\boldsymbol{e}_{2,l,fd}\boldsymbol{e}_{2,l,fd}^H] = \boldsymbol{I}_{N_{r_2}}\sigma^2_{e_{2,l,fd}}$, respectively. Here, $\sigma^2_{e_{1,fd}} = (1-\rho_1^2)\hat{\Omega}_1$ is each element's variance in $\boldsymbol{e}_{1,fd}$ and $\sigma^2_{e_{2,l,fd}} = \left(1-\rho_2^2\right)\hat{\Omega}_2$ is each element's variance in $\boldsymbol{e}_{2,l,fd}$ [34], where $\rho_v = J_0(2\pi f_{d_v})$, $0 < \rho_v < 1$, $v = 1, 2$ [35] is the time correlation coefficient of the vth hop, and f_{d_v} refers to normalized Doppler frequency of the vth hop.

In the practical case, $\boldsymbol{h}_1$ and $\boldsymbol{h}_{2,l}$ can be modelled as $\boldsymbol{h}_1 = \rho_1\hat{\boldsymbol{h}}_1^{(\tau)} + \boldsymbol{e}_{1,cee} + \boldsymbol{e}_{1,fd}$ and $\boldsymbol{h}_{2,l} = \rho_2\hat{\boldsymbol{h}}_{2,l}^{(\tau)} + \boldsymbol{e}_{2,l,cee} + \boldsymbol{e}_{2,l,fd}$ [34]. Aiming simplicity, let's define $\boldsymbol{e}_1 = \boldsymbol{e}_{1,cee} + \boldsymbol{e}_{1,fd}$ and $\boldsymbol{e}_{2,l} = \boldsymbol{e}_{2,l,cee} + \boldsymbol{e}_{2,l,fd}$ as new equivalent $N_{r_1} \times 1$ and $N_{r_2} \times 1$ vectors, respectively, where $\boldsymbol{e}_1$ is zero mean complex Gaussian random variable with $E[\boldsymbol{e}_1\boldsymbol{e}_1^H] = \boldsymbol{I}_{N_{r_1}}\sigma^2_{e_1}$ and $\boldsymbol{e}_{2,l}$ is zero mean complex Gaussian random variable with $E[\boldsymbol{e}_{2,l}\boldsymbol{e}_{2,l}^H] = \boldsymbol{I}_{N_{r_2}}\sigma^2_{e_{2,l}}$. Here, $\sigma^2_{e_1} = \sigma^2_{e_{1,cee}} + \sigma^2_{e_{1,fd}}$ is each element's variance in $\boldsymbol{e}_1$ and $\sigma^2_{e_{2,l}} = \sigma^2_{e_{2,l,cee}} + \sigma^2_{e_{2,l,fd}}$ is each element's variance in $\boldsymbol{e}_{2,l}$. Then, $\boldsymbol{h}_1 = \rho_1\hat{\boldsymbol{h}}_1^{(\tau)} + \boldsymbol{e}_1$ and $\boldsymbol{h}_{2,l} = \rho_2\hat{\boldsymbol{h}}_{2,l}^{(\tau)} + \boldsymbol{e}_{2,l}$. Now, using the new expressions of $\boldsymbol{h}_1$ and $\boldsymbol{h}_{2,l}$ in (4), the $r_{2,l}$ can be rewritten in (5), shown at the bottom of the page.

In (5), the term $r_{2,l}^S$ denotes the desired signal of U_l, $r_{2,l}^I$ represents the interference of other users, the terms $r_{2,l}^E$ demonstrate the error resulting from CEE&FD, and $r_{2,l}^N$ indicates the noise.

Recall, the hybrid diversity schemes optimal TAS/MRC is applied in the 1st and TAS-maj/MRC is applied in the 2nd hops, respectively. However, in the 1st hop, a transmit antenna at the BS, i_1, which has the maximum sum of squared channel gains between receiver antennas of the relay, is chosen. On the other hand, in the 2nd hop, a transmit antenna at the relay, i_2, which has the highest total of squared channel gains between receiver antennas for more than half of the users, is selected. According to these selection criteria, i_1 and i_2 are stated, respectively as

$$i_1 = \underset{1\le i\le N_{t_1}}{\arg\max}\left\{\varphi_1^i = \| \hat{\boldsymbol{h}}_1^{\,i} \|^2 = \sum_{j=1}^{N_{r_1}} |\hat{h}_1^{(i,j)}|^2\right\}, \tag{6}$$

$$\begin{aligned} i_2 &= \text{Maj}(i_{2,l}^*), i_{2,l}^* \\ &= \underset{1\le i\le N_{t_2}}{\arg\max}\left\{\varphi_{2,l}^i = \| \hat{\boldsymbol{h}}_{2,l}^{\,i} \|^2 = \sum_{j=1}^{N_{r_2}} |\hat{h}_{2,l}^{(i,j)}|^2\right\}, \end{aligned} \tag{7}$$

where Maj$(\cdot)$ denotes a majority function determining the majority transmit antenna [17]–[19].

C. Cooperative MIMO-NOMA Network's System Model With JTRAS Scheme

Now, similar to the TAS/MRC scheme, (1)-(5) for JTRAS scheme can also be obtained by assuming $\hat{\boldsymbol{h}}_1^{(\tau)} = \hat{h}_1^{(\tau)}$, $\hat{\boldsymbol{h}}_{2,l}^{(\tau)} = \hat{h}_{2,l}^{(\tau)}$, $\boldsymbol{w}_1 = \boldsymbol{w}_{2,l} = 1$, $\boldsymbol{e}_1 = e_1$, $\boldsymbol{e}_{2,l} = e_{2,l}$, $\boldsymbol{n}_1 = n_1$ and $\boldsymbol{n}_{2,l} = n_{2,l}$.

$$\begin{aligned} r_{2,l} = {} & \underbrace{\boldsymbol{w}_1\boldsymbol{w}_{2,l}\rho_1\rho_2\hat{\boldsymbol{h}}_1^{(\tau)}\hat{\boldsymbol{h}}_{2,l}^{(\tau)}G\sqrt{P_1P_2}\sqrt{a_l}x_l}_{r_{2,l}^S} + \underbrace{\boldsymbol{w}_1\boldsymbol{w}_{2,l}\rho_1\rho_2\hat{\boldsymbol{h}}_1^{(\tau)}\hat{\boldsymbol{h}}_{2,l}^{(\tau)}G\sqrt{P_1P_2}\sum_{i\neq l}^{L}\sqrt{a_i}x_i}_{r_{2,l}^I} + \underbrace{\boldsymbol{w}_1\boldsymbol{w}_{2,l}\boldsymbol{e}_1\boldsymbol{e}_{2,l}G\sqrt{P_1P_2}\sum_{i=1}^{L}\sqrt{a_i}x_i}_{r_{2,l}^{E1}} \\ & + \underbrace{\boldsymbol{w}_1\boldsymbol{w}_{2,l}\rho_1\hat{\boldsymbol{h}}_1^{(\tau)}\boldsymbol{e}_{2,l}G\sqrt{P_1P_2}\sum_{i=1}^{L}\sqrt{a_i}x_i}_{r_{2,l}^{E2}} + \underbrace{\boldsymbol{w}_1\boldsymbol{w}_{2,l}\rho_2\hat{\boldsymbol{h}}_{2,l}^{(\tau)}\boldsymbol{e}_1G\sqrt{P_1P_2}\sum_{i=1}^{L}\sqrt{a_i}x_i}_{r_{2,l}^{E3}} + \underbrace{\boldsymbol{w}_1\boldsymbol{w}_{2,l}\rho_2\hat{\boldsymbol{h}}_{2,l}^{(\tau)}G\sqrt{P_2}\boldsymbol{n}_1}_{r_{2,l}^{E4}} \\ & + \underbrace{\boldsymbol{w}_1\boldsymbol{w}_{2,l}\boldsymbol{e}_{2,l}G\sqrt{P_2}\boldsymbol{n}_1}_{r_{2,l}^{E5}} + \underbrace{\boldsymbol{w}_{2,l}\boldsymbol{n}_{2,l}}_{r_{2,l}^N}. \end{aligned} \tag{5}$$

As shown in Fig. 1b, the AS is done as follows: In the 1st hop, the optimal JTRAS [31] scheme is employed such that a transmit-receive antenna pair between the BS and relay, (i_1, j_1), is selected, which has the maximum channel gain between transmit antennas of BS and receiver antennas of the relay and it can be expressed as

$$(i_1, j_1) = \underset{\substack{1\le i\le N_{t_1}\\ 1\le j\le N_{r_1}}}{\arg\max}\left\{|\hat{h}_1^{(i,j)}|^2\right\}. \quad (8)$$

On the other hand, in the 2nd hop, the JTRAS-maj scheme is employed. It is realized firstly by employing the known JTRAS independently for all users. Hence, the transmit-receive antenna pair, $(i^*_{2,l}, j^*_{2,l})$, providing the maximum channel gain between the BS and U_l is determined as

$$(i^*_{2,l}, j^*_{2,l}) = \underset{\substack{i=1,\ldots,N_{t_2}\\ j=1,\ldots,N_{r_2}}}{\arg\max}\left\{|\hat{h}_{2,l}^{(i,j)}|^2\right\}, l = 1, \ldots, L. \quad (9)$$

In (9), $i^*_{2,l} \in \{1, \ldots, N_{t_2}\}$ and $j^*_{2,l} \in \{1, \ldots, N_{r_2}\}$. Next, by using Maj$(\cdot)$, the majority transmit antenna at the relay can be specified as $i_2 = \text{Maj}(i^*_{2,l})$.

III. Performance Analysis

A. Signal-to-Interference-and-Noise Ratio in Practical and Ideal Cases, and Related Statistics

Proposition 1: The expression of the instantaneous signal-to-interference-and-noise ratio (SINR) of U_l to detect the U_j, $j \neq L, j < l$, in the practical case can be derived generally for both TAS/MRC and JTRAS schemes as

$$SINR_{j\to l} = \frac{a_j\gamma^2\varphi_1\varphi_{2,l}}{\gamma^2\varphi_1\varphi_{2,l}\Sigma_j + b_1\gamma\varphi_1 + b_2\gamma\varphi_{2,l} + b_3}. \quad (10)$$

In (10), for TAS/MRC scheme $\varphi_1 = \| \hat{\boldsymbol{h}}_1^{(\tau)} \|^2 = \| \hat{\boldsymbol{h}}_1 \|^2$ and $\varphi_{2,l} = \| \hat{\boldsymbol{h}}_{2,l}^{(\tau)} \|^2 = \| \hat{\boldsymbol{h}}_{2,l} \|^2$, for JTRAS scheme $\varphi_1 = |\hat{h}_1^{(\tau)}|^2 = |\hat{h}_1|^2$ and $\varphi_{2,l} = |\hat{h}_{2,l}^{(\tau)}|^2 = |\hat{h}_{2,l}|^2$, $\gamma = \frac{P}{\sigma^2}$ is the SNR, $P = P_1 = P_2$, $\sigma^2 = \sigma_1^2 = \sigma_{2,l}^2$ and $\Sigma_j = \sum_{i=j+1}^{L} a_i$. In addition, $b_1 = \frac{\gamma\sigma_{e_{2,l}}^2+1}{\rho_2^2}$, $b_2 = \frac{\gamma\sigma_{e_1}^2+1}{\rho_1^2}$ and $b_3 = \frac{\gamma^2\sigma_{e_1}^2\sigma_{e_{2,l}}^2+\gamma\sigma_{e_{2,l}}^2+\gamma\sigma_{e_1}^2+1}{\rho_1^2\rho_2^2}$. If $\rho_1 = \rho_2 = 1$ and $\sigma_{e_1}^2 = \sigma_{e_{2,l}}^2 = 0$, then $b_1 = b_2 = b_3 = 1$. Hence, by substituting bs into (10), the instantaneous $SINR_{j\to l}$'s expression in the ideal case is obtained. Note that Proof of Proposition 1 is given in Appendix A.

Magnitudes of the fading gains are identically and independently distributed (i.i.d.) with Nakagami-*m* distribution. By the help of the series expansion of incomplete Gamma function [37, eq.(8.352.6)], lower incomplete Gamma function [37, eq.(8.350.1)], eq.(8.350.1)], and Gamma function [37, eq.(8.310.1)], the CDF and PDF of Gamma random variable X, which is the square of random variable can be defined, respectively

$$F_X(x) = \frac{\Psi(m_x, \frac{m_x x}{\Omega_x})}{\Gamma(m_x)} = 1 - e^{-\frac{m_x x}{\Omega_x}}\sum_{k=0}^{m_x-1}(\frac{m_x x}{\Omega_x})^k\frac{1}{k!}, \quad (11)$$

$$f_X(x) = (\frac{m_x}{\Omega_x})^{m_x}\frac{x^{m_x-1}}{\Gamma(m_x)}e^{-\frac{m_x x}{\Omega_x}}. \quad (12)$$

In (11) and (12), m_x is the Nakagami-*m* distribution's parameter as well as $\Omega_x = E[|X|^2]$.

By assuming i.i.d. random variables, using binomial expansions and series with assistance of multinomial coefficients, CDF $F_{\varphi_1}(x)$ is written

$$F_{\varphi_1}(x) = \left(\frac{\Psi(m_1, \frac{m_1\beta_{r_1}x}{\Omega_1})}{\Gamma(m_1\beta_{r_1})}\right)^{\beta_{t_1}} = \sum_{p=0}^{\beta_{t_1}}\sum_{k=0}^{p(m_1\beta_{r_1}-1)}\binom{\beta_{t_1}}{p} \times(-1)^p\vartheta_k(p, m_1\beta_{r_1})x^k e^{-\frac{pm_1x}{\Omega_1}}. \quad (13)$$

In (13), for TAS/MRC scheme $\{\beta_{r_1}, \beta_{t_1}\} = \{N_{r_1}, N_{t_1}\}$, for JTRAS scheme $\{\beta_{r_1}, \beta_{t_1}\} = \{1, N_{r_1}N_{t_1}\}$ and $\vartheta_x(y, g_z)$ refers to multinomial coefficients, where $\vartheta_x(y, g_z) = \frac{1}{xd_0}\sum_{w=1}^{x}(w(y+1)-x)d_w\vartheta_{x-y}(y, g_z)$, $x \geq 1$ [37, eq.(0.314)]. Here, $d_w = (g_z/\Omega_z)^w/w!$, $\vartheta_0(y, g_z) = 1$, and $\vartheta_x(y, g_z) = 0$ if $w > g_z - 1$. In order to avoid the heavy load of the complexity and undecided states of the majority algorithm [17]–[19], we assume $N_{t_2} = 2$ and $L = 3$. So, using [18], generally the CDF and PDF $F_{\varphi_{2,l}}(x)$ are expressed, respectively as

$$\begin{aligned} F_{\varphi_{2,l}}(x) &= \sum_{q=1}^{3\beta_{t_2}}\zeta_{(l,q)}\left(\frac{\Psi(m_2\beta_{r_2}, \frac{m_2x}{\hat{\Omega}_2})}{\Gamma(m_2\beta_{r_2})}\right)^{q\beta} \\ &= \sum_{q=1}^{3\beta_{t_2}}\zeta_{(l,q)}\left(1 - e^{-\frac{m_2x}{\hat{\Omega}_2}}\sum_{s=0}^{m_2\beta_{r_2}-1}(\frac{m_2x}{\hat{\Omega}_2})^s\frac{1}{s!}\right)^{q\beta}, \end{aligned} \quad (14)$$

$$\begin{aligned} f_{\varphi_{2,l}}(x) &= \sum_{q=1}^{3\beta_{t_2}} q\beta\zeta_{(l,q)}\frac{(m_2/\hat{\Omega}_2)^{m_2\beta_{r_2}}}{\Gamma(m_2\beta_{r_2})} \\ &\times\left(1 - e^{-\frac{m_2x}{\hat{\Omega}_2}}\sum_{s=0}^{m_2\beta_{r_2}-1}(\frac{m_2x}{\hat{\Omega}_2})^s\frac{1}{s!}\right)^{q\beta-1} \\ &\times x^{m_2\beta_{r_2}-1}e^{-\frac{m_2x}{\hat{\Omega}_2}}. \end{aligned} \quad (15)$$

where $\{\beta_{r_2}, \beta_{t_2}, \beta\} = \{N_{r_2}, N_{t_2}, 1\}$ for TAS/MRC scheme, $\{\beta_{r_2}, \beta_{t_2}, \beta\} = \{1, N_{t_2}, N_{r_2}\}$ for JTRAS scheme, $\zeta_{(1,1)} = \zeta_{(1,2)} = \frac{3}{2}, \zeta_{(1,3)} = -\frac{9}{2}, \zeta_{(1,4)} = \frac{15}{4}, \zeta_{(1,5)} = -\frac{3}{2}, \zeta_{(1,6)} = \frac{1}{4}, \zeta_{(2,3)} = 3, \zeta_{(2,4)} = -\frac{3}{4}, \zeta_{(2,5)} = -\frac{9}{4}, \zeta_{(2,6)} = 1, \zeta_{(3,5)} = \frac{3}{2}, \zeta_{(3,6)} = -\frac{1}{2}$ and otherwise equal zero. Thus, using series and binomial expansions with assistance of multinomial coefficients, $f_{\varphi_{2,l}}(x)$ is

$$\begin{aligned} &f_{\varphi_{2,l}}(x) \\ &= \sum_{q=1}^{3\beta_{t_2}}\zeta_{(l,q)}q\beta\left(\frac{\Psi(m_2\beta_{r_2}, \frac{m_2x}{\hat{\Omega}_2})}{\Gamma(m_2\beta_{r_2})}\right)^{q\beta-1} \\ &\times\frac{(m_2/\hat{\Omega}_2)^{m_2\beta_{r_2}}}{\Gamma(m_2\beta_{r_2})}x^{m_2\beta_{r_2}-1}e^{-\frac{m_2x}{\hat{\Omega}_2}} \\ &= \frac{(m_2/\hat{\Omega}_2)^{m_2\beta_{r_2}}}{\Gamma(m_2\beta_{r_2})}\sum_{q=1}^{3\beta_{t_2}}\sum_{t=0}^{q\beta-1}\sum_{s=0}^{t(m_2\beta_{r_2}-1)}\binom{q\beta-1}{t}(-1)^t \\ &\times q\beta\zeta_{(l,q)}\vartheta_s(t, m_2\beta_{r_2})x^{m_2\beta_{r_2}+s-1}e^{-\frac{m_2(t+1)x}{\hat{\Omega}_2}}. \end{aligned} \quad (16)$$

B. OP in Practical and Ideal Cases

According to the OP's definition and by using (10), the OP_l can be driven as

$$\begin{aligned} OP_l &= P_r(SINR_{j\to l} < \gamma_{th_j}) \\ &= P_r\left(\varphi_1 < \frac{\theta_l^*(b_2\gamma\varphi_{2,l} + b_3)}{\gamma(\varphi_{2,l} - b_1\theta_l^*)}\right). \end{aligned} \tag{17}$$

Proposition 2: For both TAS/MRC and JTRAS schemes, the OP of the U_l in the practical case can be expressed in closed-form as

$$\begin{aligned} OP_l = 1 + 2&\frac{(m_2/\hat{\Omega}_2)^{m_2\beta_{r_2}}}{\Gamma(m_2\beta_{r_2})} \sum_{q=1}^{3\beta_{t_2}} \sum_{t=0}^{q\beta-1} \sum_{s=0}^{t(m_2\beta_{r_2}-1)} \sum_{p=1}^{\beta_{t_1}} \\ &\times \sum_{k=0}^{p(m_1\beta_{r_1}-1)} \sum_{k_1=0}^{m_2\beta_{r_2}+s-1} \sum_{k_2=0}^{k} \binom{q\beta-1}{t}\binom{\beta_{t_1}}{p} \\ &\times \binom{m_2\beta_{r_2}+s-1}{k_1}\binom{k}{k_2}(-1)^{t+p} q\beta\zeta_{(l,q)} \\ &\times \vartheta_s(t, m_2\beta_{r_2})\vartheta_k(p, m_1\beta_{r_1}) \\ &\times (\frac{\theta_l^*}{\gamma})^k e^{-\frac{m_2 b_1\theta_l^*(t+1)}{\hat{\Omega}_2}} e^{-\frac{pm_1 b_2\theta_l^*}{\hat{\Omega}_1}} \\ &\times (b_1\theta_l^*)^{m_2\beta_{r_2}+s-1-k_1}(\gamma b_1 b_2\theta_l^* + b_3)^{k-k_2} \\ &\times (\gamma b_2)^{k_2}(\frac{c_1}{c_2})^{\frac{k_1+k_2-k+1}{2}} K_{k_1+k_2-k+1}(2\sqrt{c_1 c_2}). \end{aligned} \tag{18}$$

In (18), $\theta_l^* = \max_{1\le j\le l}\left\{\frac{\gamma_{th_j}}{\gamma\left(a_j - \gamma_{th_j}\Sigma_j\right)}\right\}$, γ_{th_j} refers to the SNR's threshold value for the U_j with $a_j > \gamma_{th_j}\Sigma_j$. $K_u(.)$ denotes the uth order of modified Bessel function of the second kind [37], eq.(3.471.9)], $c_1 = \frac{pm_1\theta_l^*(\gamma b_1 b_2\theta_l^* + b_3)}{\gamma\hat{\Omega}_1}$ and $c_2 = \frac{m_2(t+1)}{\hat{\Omega}_2}$. By substituting $b_1 = b_2 = b_3 = 1$ into (18), the OP of the U_l in the ideal case can be obtained. Proof of Proposition 2 is given in Appendix B.

C. Lower Bound OP in Practical Case

Using (17), OP_l can be rewritten as

$$\begin{aligned} OP_l &= P_r\left(\frac{\frac{\gamma}{b_3}\varphi_1\varphi_{2,l}}{\frac{b_1}{b_3}\gamma\varphi_1 + \frac{b_2}{b_3}\gamma\varphi_{2,l} + 1} < \theta_l^*\right) \\ &= 1 - P_r\left(\frac{\frac{\gamma b_1}{b_3}\varphi_1\frac{\gamma b_2}{b_3}\varphi_{2,l}}{\frac{\gamma b_1}{b_3}\varphi_1 + \frac{\gamma b_2}{b_3}\varphi_{2,l} + 1} \ge \frac{\gamma b_1 b_2}{b_3}\theta_l^*\right). \end{aligned} \tag{19}$$

By using the inequality $\frac{ab}{a+b+1} \le \min(a,b)$ [38], the lower bound of OP, $OP_{l,LB}$, is given by

$$\begin{aligned} OP_{l,LB} &= 1 - P_r\left(\min(\frac{\gamma b_1}{b_3}\varphi_1, \frac{\gamma b_2}{b_3}\varphi_{2,l}) \ge \frac{\gamma b_1 b_2}{b_3}\theta_l^*\right) \\ &= F_{\varphi_1}(b_2\theta_l^*) + F_{\varphi_{2,l}}(b_1\theta_l^*) - F_{\varphi_1}(b_2\theta_l^*)F_{\varphi_{2,l}}(b_1\theta_l^*). \end{aligned} \tag{20}$$

After substituting (13) and (14) into (20), the expression for the $OP_{l,LB}$ is obtained.

D. EF in Practical Case

By defining $\zeta_l = \max_{1\le j\le l}(\frac{\gamma_{th_j}}{a_j - \gamma_{th_j}\Sigma_j})$, then $\theta_l^* = \frac{\zeta_l}{\gamma}$. Thus, in the high SNR region

$$b_2\theta_l^* = \frac{\sigma_{e_1}^2\zeta_l}{\rho_1^2}, \qquad b_1\theta_l^* = \frac{\sigma_{e_{2,l}}^2\zeta_l}{\rho_2^2}. \tag{21}$$

By substituting (21) into (20), then the lower bound of the EF, $EF_{l,LB}$, can be given in the high SNR region by

$$\begin{aligned} EF_{l,LB} = F_{\varphi_1}\left(\frac{\sigma_{e_1}^2\zeta_l}{\rho_1^2}\right) + F_{\varphi_{2,l}}\left(\frac{\sigma_{e_{2,l}}^2\zeta_l}{\rho_2^2}\right) \\ - F_{\varphi_1}\left(\frac{\sigma_{e_1}^2\zeta_l}{\rho_1^2}\right)F_{\varphi_{2,l}}\left(\frac{\sigma_{e_{2,l}}^2\zeta_l}{\rho_2^2}\right). \end{aligned} \tag{22}$$

After substituting (13) and (14) into (22), the expression for the $EF_{l,LB}$ is obtained. It is observed from (22) that the $EF_{l,LB}$ does not depend on the γ. Thus, the OP reaches a fixed value in the high SNR region, which indicates that the diversity order is zero in the practical case.

E. Asymptotic OP in Ideal Case

In the ideal case, bs in (20) are equal to 1 and then by using [39], $\gamma \to \infty$, then $\theta_l^* \to 0$. Besides, using $\Psi(x, y \to 0) \approx y^x/x$ [40], asymptotic expressions $F_{\varphi_1}^{\infty}(\theta_l^*)$ and $F_{\varphi_{2,l}}^{\infty}(\theta_l^*)$ can be expressed, respectively as

$$\begin{aligned} F_{\varphi_1}^{\infty}(\theta_l^*) &= \frac{\left(\frac{m_1\theta_l^*}{\Omega_1}\right)^{m_1\beta_{t_1}\beta_{r_1}}}{\Gamma(m_1\beta_{r_1}+1)^{\beta_{t_1}}} \\ &= \frac{(m_1/\Omega_1)^{m_1\beta_{t_1}\beta_{r_1}}}{\Gamma(m_1\beta_{r_1}+1)^{\beta_{r_1}}}(\theta_l^*)^{m_1\beta_{t_1}\beta_{r_1}}, \end{aligned} \tag{23}$$

$$\begin{aligned} F_{\varphi_{2,l}}^{\infty}(\theta_l^*) &= \sum_{q=1}^{3\beta_t}\zeta_{(l,q)}\left(\frac{(m_2/\Omega_2)^{m_2\beta_{r_2}}}{\Gamma(m_2\beta_{r_2}+1)}(\theta_l^*)^{m_2\beta_{r_2}}\right)^{q\beta} \\ &= \sum_{q=1}^{3\beta_{t_2}}\zeta_{(l,q)}\frac{(m_2/\Omega_2)^{q\beta m_2\beta_{r_2}}}{\Gamma(m_2\beta_{r_2}+1)^{q\beta}}(\theta_l^*)^{q\beta m_2\beta_{r_2}}. \end{aligned} \tag{24}$$

After substituting (23) and (24) into (20), the expression for the $OP_{l,asym}$ is obtained. It is observed that the $OP_{l,asym}$ depends on γ. Hence, the non-zero diversity and array gains are achieved in ideal case.

IV. TEST-BED

In the OP measurements for dual-hop 3-User MIMO NOMA system as shown in Fig. 2, a total of 5 USRP model SDR units, including 1 transmitter, 1 relay and 3 users, are used. Two USRP-2901 models are used for the transmitter source and relay, while 3 identical USRP-2943Rs are selected as users at the receiving end. The BS, relay and receiver radios have double RF channels and each channel has a transmitter and receiver. Thus, each antenna has become independent from each other by connecting different channels.

LabVIEW, a graphical modeling and design tool, is used to program the SDRs and conduct tests. As shown in Fig. 2, in order to prevent deceleration in data processing speed due to overloaded processors, real-time test environment set up with

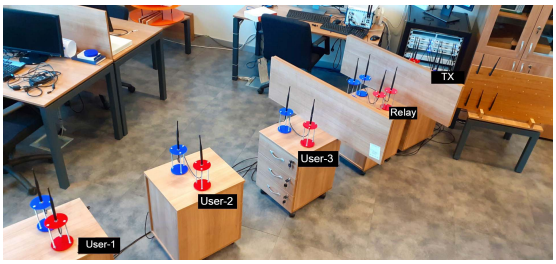

Fig. 2. A picture of the designed test-bed using three USRP-2943Rs. The NOMA users are indicated as User-1, User-2 and User-3, respectively.

TABLE II
DETAILS OF THE TEST CONFIGURATION

Parametesrs		**Values**
Modulation		BPSK
Carrier Frequency		2.11 GHz
Bandwidth		400 KHz
I/Q Data Rate		500 kS/sec
Channel Fading of Test-1 and Test-2		Nakagami, *m*= 0.98, *m*= 5.26
Power Coefficients (far to near)		0.761, 0.191, 0.048
Transmitter Gain		0-30 dB
Receiver Gain		20 dB
Threshold Values (far to near)		2.8, 3.0, 3.0
Number of Antennas	Transmitter	2
	Relay	4
	Users	2
Distance from Relay	U_3	0.8 m
	U_2	1.6 m
	U_1	2.4 m

the transmitter radio connected to a desktop computer, the relay connected to a PXIe-1082 chassis and 3 users connected to a PXIe-1085 chassis. User antennas are placed with 80 cm intervals using 5 meter long SMA cables. An OctoClock-G CDA-2990 has been used as a high accuracy timing reference among users in order to minimize hardware impairment effects. USRP 2901 used for the source and relay has a maximum bandwidth of 56 MHz and an operating range of 70 MHz to 6 GHz. Details of the test configuration are given in Table II. In addition to that, USRP-2943R, which is used for the users, has a maximum 40 MHz band range in the 1.2 GHz to 6 GHz operating range. The carrier frequency of the test system is 2.11 GHz and the bandwidth is 800 KHz. BPSK modulated single carrier wave frame is constructed on the BS consists of a 64-bit long preamble, 17 bits of uniform regular pilot tones and 128 bits of data signals. Meanwhile, data consists of a superpositioned of each sequence multiplied by a power coefficient of the user to whom it is assigned. Moreover, the matched filter is applied as a linear filter to minimize noise at the transmitter output and receiver input. 2 silicon coated wooden panels of 1m $\times$ 4m size are placed between the BS-relay and relay-users to obstruct line of sight and create Rayleigh channel distribution in both hops. Along with the tests, maximum likelihood estimate of Nakagami-*m* factor is estimated as 0.98 using the channel coefficients. Antenna selection procedures are also carried out with the same coefficients. Both the JTRAS and the TAS/MRC configurations have been implemented as detailed below.

- *JTRAS Configuration:* Before starting the tests, a trial run was conducted to determine the antennas. While the best channel gain between the relay and the BS is used for BS transmitter and relay receiver antenna selections, relay transmitter antenna is determined using the channel gains between the relay and users according to the majority rule as picking the better antenna for more than half of the users after finding the best link between the relay and each user. The tests started with the completion of the antenna selection process.
- *TAS/MRC Configuration:* In the TAS/MRC configuration, with all parameters being the same as JTRAS method, except antenna selection method. First optimal TAS used between BS and relay, and then majority based TAS is used for relay between the relay and users. MRC method is used in 2-channel receivers of the relay and each user. It was ensured that the receiver antennas could capture identical frames in users and relay. During the tests, users' data and SNR values were recorded and changes in antenna selection methods were observed. the following signal processing steps then applied for both configurations.

As the first hop of data transfer, the transmitted frame reaches the relay and the amplified signal is directed towards the users. In the second hop, firstly symbol timing offset (STO), and then carrier frequency offset (CFO) estimations and compensations are performed at the receiver using repeated preambles. Thus, synchronization processes are completed. The pilot tones that are uniformly inserted to the frame are used to estimate channel status with the linear regression approach in order to equalize the distorted received data using zero forcing method. After equalization and synchronization, users obtain their own data by passing the superpositioned signal through the SIC algorithm determined at different levels with respect to the user.

Note that due to the nature of the SDR-based tests, OPs are captured through the estimated link SNR values. In the premises, while the User-3 passes through 2-level SIC and User-2 single-level SIC, User-1 does not get into SIC operation. Each receiver performs outage analysis by comparing the SNR values with the threshold value determined by the obtained bit number per second. For this purpose, SNR of the received signal is estimated by using the repetitive preamble added to the beginning of each symbol sent. The SNR value is obtained by proportioning the power of the received signals in the sequence to the noise power, which is the power of the differences of the repetitive identical signals. Eventually, the ratio of number of cases with outage to the total number of cases gives instantaneous OP value.

V. NUMERICAL RESULTS

In this section, we present some numerical and SDR test results for the OP performance of the cooperative MIMO-NOMA network in order to illustrate effect of the antenna configuration, channel condition, CEE and FD on the system performance. As well, a comparison of the proposed AS schemes with the previous ones. In all theoretical and simulation results, unless otherwise stated, we assume $\Omega = 1$, $d_1 = d_2 = 0.5$, the power allocation coefficients of the three users and their threshold SINR values as

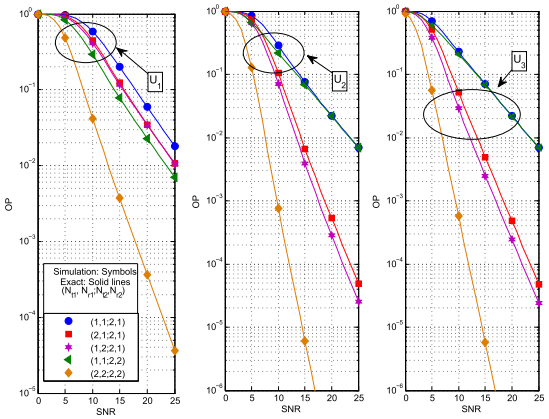

Fig. 3. OP vs SNR for TAS/MRC scheme in the ideal case with different antenna configurations.

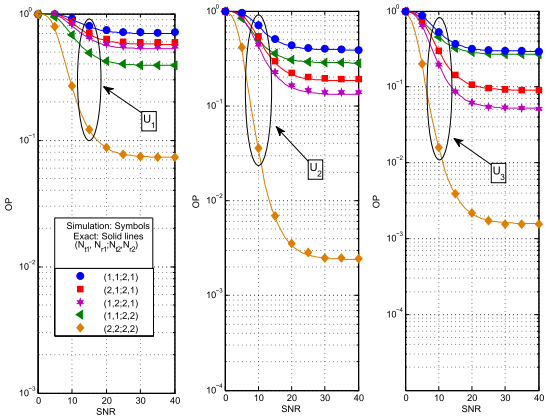

Fig. 4. OP vs SNR for TAS/MRC scheme in the practical case with different antenna configurations.

$(a_1, \gamma_{th_1}) = (0.6, 1.4)$ $(a_2, \gamma_{th_2}) = (0.3, 2.2)$ and $(a_3, \gamma_{th_3}) = (0.1, 2.5)$ unless otherwise stated. In addition, the parameters $(\sigma^2_{e,cee}, f_d)$ are considered as $(0, 0)$ and $(0.002, 0.02)$ for the ideal and practical cases, respectively unless otherwise stated. In all figures, SNR values are given in dB scale.

To see the effect of the antenna configuration and channel condition on the OP for the TAS/MRC scheme, the OP versus SNR in the absence and presence of CEE&FD cases are plotted in Fig. 3 and Fig. 4, respectively with a special case Rayleigh fading channel is assumed in both hops, i.e., $(m_1, m_2) = (1, 1)$ and different transmit/receive antennas. On the other hand, Fig. 5 presents the OP versus SNR for both cases, absence and presence of CEE&FD with different channel conditions and a special antenna configuration, i.e., TAS and TAS-maj schemes are employed at the 1st and 2nd hops, respectively for $N_{t1} = N_{t2} = 2$. From Fig. 3-Fig. 5, we notice that the analytical matches the simulation results completely. Besides, the OP performance enhances as the number of transmit and/or receive antennas increases and channel condition improves. In particular, the performance of U_1 improves better when the number of the receive antennas of the 2nd hop increases rather than when the numbers of the transmit and/or receive antennas of the 1st hop increase. For example, in Fig. 3, to achieve OP of 10^{-1} for U_1, there are approximately 3 dB and 5 dB SNR gain advantages for $(N_{t1}, N_{r1}; N_{t2}, N_{r2}) = (2, 1; 2, 1)/(1, 2; 2, 1)$

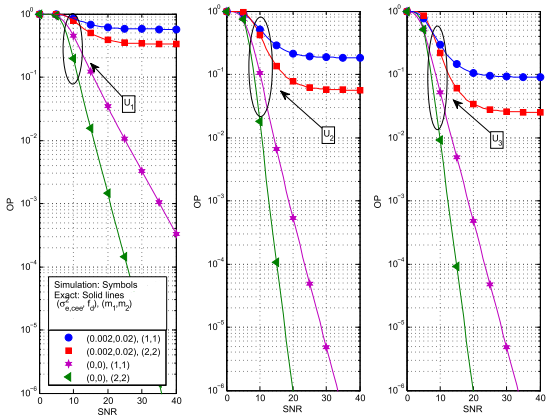

Fig. 5. OP vs SNR for TAS/MRC scheme in the ideal and practical cases with different channel conditions.

over $(1, 1; 2, 1)$, and $(1, 1; 2, 2)$ over $(1, 1; 2, 1)$, respectively. Therefore, $(1, 1; 2, 2)$ achieves 2 dB SNR gain advantage over $(2, 1; 2, 1)/(1, 2; 2, 1)$. On the other hand, the performance of the U_2 and U_3 considerably enhances when the numbers of the transmit and/or receive antennas of the 1st hop increase. For example, to achieve OP of 10^{-2} for U_2, there are approximately 9 dB and 10 dB SNR gain advantages for $(2, 1; 2, 1)$ and $(1, 2; 2, 1)$, respectively over $(1, 1; 2, 1)$. As well, to achieve OP of 10^{-2} for U_3, there are approximately 10 dB and 11.5 dB SNR gain advantages for $(2, 1; 2, 1)$ and $(1, 2; 2, 1)$, respectively over $(1, 1; 2, 2)/(1, 1; 2, 1)$. Meanwhile, in Fig. 5, to achieve OP of 10^{-3} for U_1, U_2 and U_3 there are approximately 15 dB, 6 dB and 6 dB SNR gain advantages for $(m_1, m_2) = (2, 2)$ over $(1, 1)$, respectively in the ideal case. Obviously, we notice from Fig. 4 and Fig. 5, the CEE&FD's impact on the OP performance as the OP performance degrades in the practical case while in the ideal case better OP performance is obtained. For the sake of clarity, the asymptotic curves, the corresponding lower bound, and EF of only U_1 for the TAS/MRC scheme are shown in the left and right of Fig. 6, respectively for different parameters of antenna configurations and channel conditions. As depicted in Fig. 6, the asymptotic curves are compatible with the exact ones, and the diversity and array gains are achieved in the ideal case. On the other hand, the OP reaches an EF due to CEE&FD when the system SNR increases, which means zero-diversity order is achieved. It is notable to mention that although CEE&FD affect the OP performance, the EF can be reduced by having more array gain with larger number of antennas or having better channel conditions.

Fig. 7 illustrates the performance of the OP versus $\sigma^2_{e,cee}$ and f_d for the TAS/MRC scheme. The parameters of antenna configuration and channel condition labeled as $(m_1, N_{t1}, N_{r1}; m_2, N_{t2}, N_{r2}) = (1, 2, 2; 1, 2, 2)$. It is observed that the OP performance gets worse as CEE or FD increases. Nevertheless, for any user the OP converges to the same value with the increase of FD or CEE for different SNR values.

Fig. 8-Fig. 10 depict the OP performance versus d_1 for the TAS/MRC scheme with different values of $(\sigma^2_{e,cee}, f_d)$, $(N_{t1}, N_{r1}; N_{t2}, N_{r2})$, and (m_1, m_2), respectively. We assume SNR = 15 dB in Fig. 8-Fig. 10, the parameters of antenna configuration and channel condition are labeled as

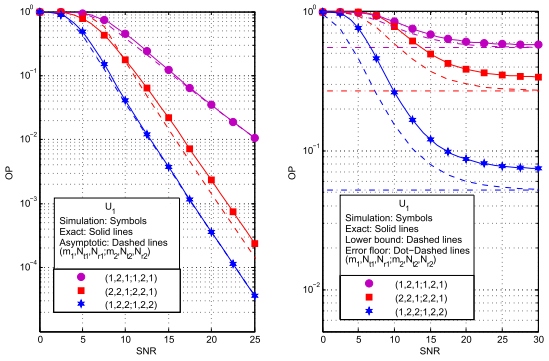

Fig. 6. Asymptotic OP, lower bound OP and EF vs SNR for the TAS/MRC scheme.

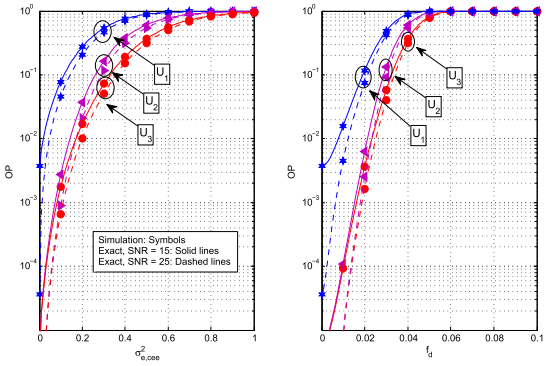

Fig. 7. OP vs $\sigma^2_{e,cee}$ and f_d for the TAS/MRC scheme.

$(m_1, N_{t1}, N_{r1}; m_2, N_{t2}, N_{r2}) = (1,2,2;1,2,2)$ in Fig. 8, $(m_1, m_2) = (1,1)$ in Fig. 9 and $(N_{t1}, N_{r1}; N_{t2}, N_{r2}) = (2,1;2,1)$ in Fig. 10. Furthermore, in order to compare NOMA with conventional OMA, the threshold SNR value of the conventional OMA γ_{th}, which verifies $\frac{1}{2}\sum_{i=1}^{L}\log_2(1+\gamma_{th_i}) = \frac{1}{2}\log_2(1+\gamma_{th})$ [24], is used and then $\gamma_{th} = 25.88$ is obtained. As shown in Fig. 8, the optimal location of the relay becomes closer to the middle for all users in the practical case as compared to that in the ideal case. Fig. 8 shows that the NOMA is superior to conventional OMA when the location of the relay is closer to BS. Moreover, performance of conventional OMA is better than NOMA when the location of the relay is closer to users but NOMA provides better user fairness and higher spectral efficiency. In addition, it is noticed from Fig. 9 that the optimal location of the relay becomes nearer to the BS when the number of the antennas of the 2nd hop (N_{t2}, N_{r2}) increases, whereas from Fig. 10 it becomes closer to the users when the channel condition of the 1st hop (m_1) increases.

Fig. 11 represents the OP performance versus the value of a_2 (power allocation coefficient of the U_2) in the case of ideal and practical conditions with $(m_1, N_{t1}, N_{r1}; m_2, N_{t2}, N_{r2}) = (1,2,2;1,2,2)$. With the predetermined conditions of $\sum_{i=1}^{L} a_i = 1$ and $a_l > \gamma_{th_l}\sum_{i=l+1}^{L} a_i$, the effective range of power allocation coefficient in order to achieve optimum OP performance for the U_1 can be found as $a_1 > \gamma_{th_1}(a_2 + a_3)$. As $a_2 + a_3 = 1 - a_1$, then $a_1 > \gamma_{th_1}(1-a_1) = \gamma_{th_1} - a_1\gamma_{th_1}$. Accordingly, $a_1 > \frac{\gamma_{th_1}}{1+\gamma_{th_1}}$. Similarly, the effective range of power allocation coefficient for the U_2 and U_3 can be stated, respectively as $a_2 > \frac{(1-a_1)\gamma_{th_2}}{1+\gamma_{th_2}}$ and $0 < a_3 < \frac{1-a_1}{1+\gamma_{th_2}}$.

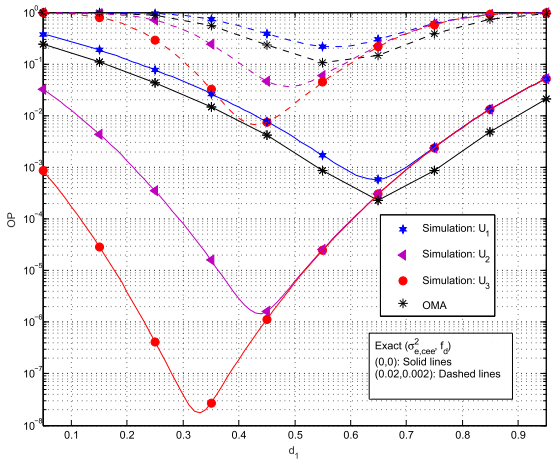

Fig. 8. OP vs d_1 for the TAS/MRC scheme with different values of $(\sigma^2_{e,cee}, f_d)$.

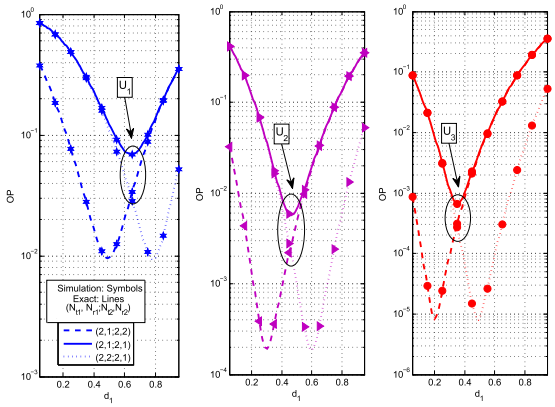

Fig. 9. OP vs d_1 for the TAS/MRC scheme with different values of $(N_{t1}, N_{r1}; N_{t2}, N_{r2})$.

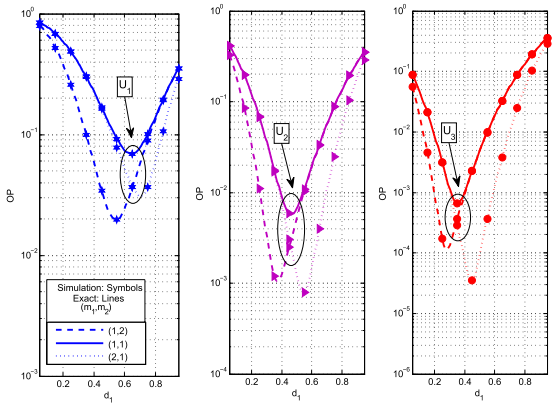

Fig. 10. OP vs d_1 for the TAS/MRC scheme with different values of (m_1, m_2).

Also, the optimum power allocation coefficient of U_1 is set as $a_1 = \frac{6}{10}$ due to the given target SINRs. From the figure, the effective range of power allocation coefficient for the U_2 and U_3 can be found, respectively as $a_2 > 0.275$ and $0 < a_3 < 0.125$. Besides, the optimum power allocation coefficients for the U_2 and U_3 are observed as $a_2 = \frac{3}{10}$ and $a_3 = \frac{1}{10}$ due to the given target SINRs. As well, it can be clearly seen that CEE and FD worsen the OP performance of all users.

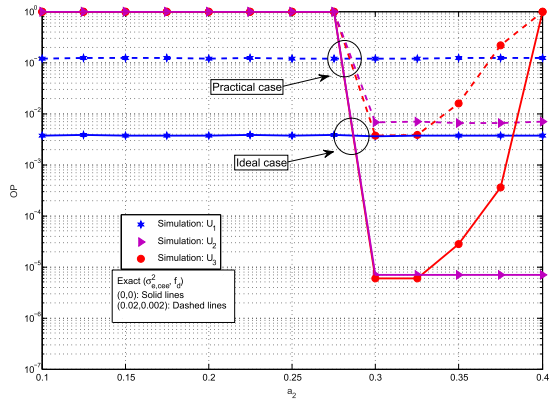

Fig. 11. OP versus a_2.

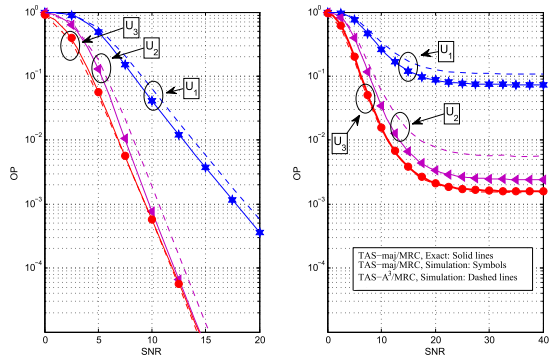

Fig. 12. A comparison between TAS-maj/MRC and TAS-A^3/MRC in ideal and practical cases.

Fig. 12 and Fig. 13 provide a comparison between the proposed AS schemes and the previous ones [20]–[22] in the absence and presence of CEE&FD in the left and right of these figures, respectively. For both figures, we assume that the optimal TAS/MRC scheme is employed in the 1st hop while in the 2nd hop, the suboptimal schemes TAS-maj/MRC, TAS-A^3/MRC and TAS-AIA/MRC are employed. In Fig. 12 and Fig. 13, the OP performance of the TAS-maj/MRC scheme is compared to those of the TAS-A^3/MRC and TAS-AIA/MRC schemes, respectively with $(m_1, N_{t1}, N_{r1}; m_2, N_{t2}, N_{r2}) = (1, 2, 2; 1, 2, 2)$. We notice from Fig. 12 that the TAS-maj/MRC scheme superiors to the TAS-A^3/MRC scheme for U_1 and U_2 and approximately they have the same performance for U_3. For example, for the U_1 and U_2, at an OP of 10^{-3}, the TAS-maj/MRC scheme accomplishes approximately 2 dB SNR gain as compared to the TAS-A^3/MRC scheme in the absence of CEE&FD. On the other hand, in Fig. 13, we see that the TAS-maj/MRC and TAS-AIA/MRC provide similar OP performance enhancement to the users. In other words, each AS scheme offers better performance for one user than the other scheme; the TAS-maj/MRC provides better performance for U_2 while TAS-AIA/MRC scheme offers better performance for U_1 and both schemes have the same performance for U_3. In summary, although A^3 based AS scheme in [20]–[22] is designed to enhance the strong user's (U_3), as shown in Fig. 12, the TAS-A^3 provides the same performance for U_3 and does not have the superiority over the TAS-maj/MRC. In contrast, the TAS-maj/MRC offers better performance for two users

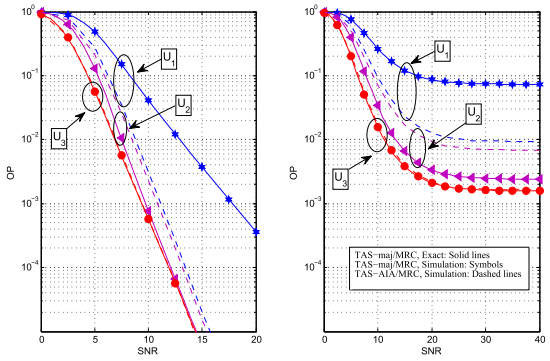

Fig. 13. A comparison between TAS-maj/MRC and TAS-AIA/MRC in ideal and practical cases.

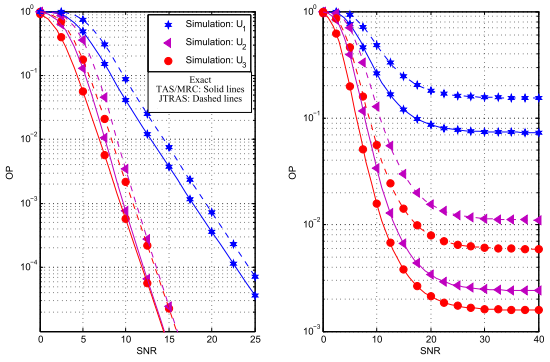

Fig. 14. OP vs SNR for the TAS/MRC and JTRAS schemes in the ideal and practical cases.

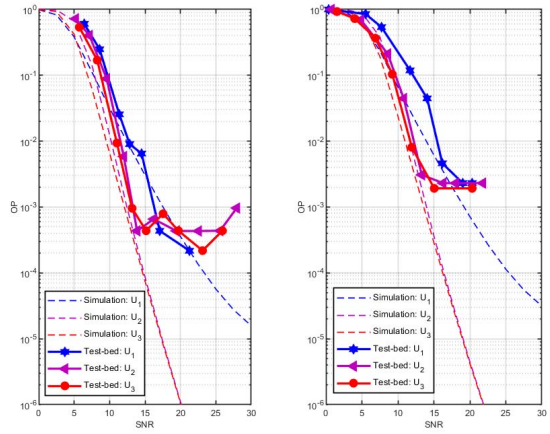

Fig. 15. OP vs SNR for the TAS/MRC and JTRAS schemes with SDR in the practical case.

(U_1 and U_2). In addition, the TAS-maj/MRC still has no preference over TAS-AIA/MRC scheme. Moreover, as shown in Fig. 12 and Fig. 13, for U_1 and U_2 in the practical case, the difference in the performance between the TAS-maj/MRC and TAS-A^3/MRC or TAS-AIA/MRC schemes increases. *It is worth mentioning that for the sake of brevity, we merely demonstrated the OP of the TAS/MRC scheme in Fig. 3-13. Nevertheless, all the interpretations noticed in Fig. 3-13 are also true for JTRAS scheme.*

The OP performances of the majority-based AS schemes are compared in the absence and presence of CEE&FD in left and right of Fig. 14, respectively. In addition, Fig. 15 demonstrates the OP performances of both schemes through the SDR-based SDR-based real-time tests. In Fig. 14 and Fig. 15,

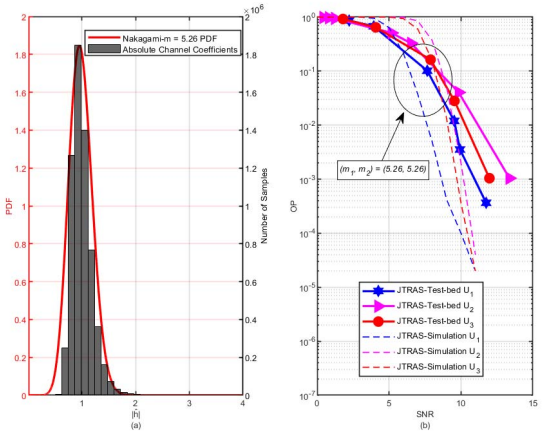

Fig. 16. (a) Absolute distributions of the channel coefficients recorded in the first and second hops. (b) JTRAS tests when $(m_1, m_2) = (5.26, 5.26)$.

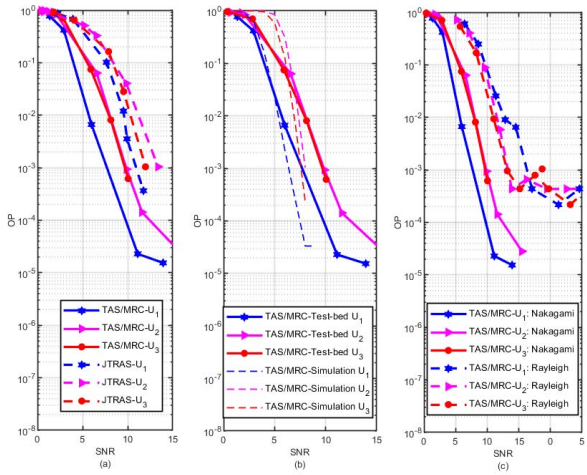

Fig. 17. (a) A comparison between JTRAS and TAS/MRC tests when $(m_1, m_2) = (5.26, 5.26)$. (b) A comparison between results of TAS/MRC tests and simulations when $(m_1, m_2) = (5.26, 5.26)$. (c) A comparison of TAS/MRC tests with different (m_1, m_2).

the parameters of antenna configuration and channel condition labeled as $(m_1, N_{t1}, N_{r1}; m_2, N_{t2}, N_{r2}) = (1, 2, 2; 1, 2, 2)$. In Fig. 14, the power allocation coefficients of the three users and their threshold SINR values are assumed as before however, in Fig. 15, they are labeled as $(0.761, 2.8)$ $(a_2, \gamma_{th_2}) = (0.191, 3)$ and $(a_3, \gamma_{th_3}) = (0.048, 3)$, and the parameters parameters $(\sigma^2_{e,cee}, f_d)$ are considered as $(0.0014, 0)$. As seen from Fig. 14, the superiority of TAS-maj/MRC over the JTRAS-maj scheme such as the TAS-maj/MRC scheme in the ideal case provides approximately 2 dB SNR gain at an OP of 10^{-2} for all users as compared to JTRAS-maj scheme. Also, the TAS-maj/MRC scheme in the practical case offers approximately 7.5 dB approximately 7.5 dB SNR gain at an OP of 10^{-2} for U_3, for example. As seen in Fig. 15, the test results have a the theoretical curves up to some SNR values, then diverge and EF, frequently encountered in real-time tests appears as a result of estimation processes. This floor is observed due to the composite effect of the real-time design related impairments.

The absolute distributions of the channel coefficients recorded in the first hop in the barrier-free tests are given in Fig. 16-(a). It is assumed that the second hop also has the same distribution. With the maximum likelihood estimation (MLE) method, it is assumed that the Nakagami distribution converges to the *m* factor of 5.26. Using the curve fitting technique, it was determined that the Nakagami-*m* factor of this distribution was approximately 5.26, therefore this value was used in simulations. Unlike the previously set Rayleigh channel tests, the JTRAS tests in Fig. 16-(b) have taken with the silicon panel removed and the channel predicted to be the Nakagami channel. Here, we assume the parameters as $(m_1, N_{t1}, N_{r1}; m_2, N_{t2}, N_{r2}) = (5.26, 2, 2; 5.26, 2, 2)$, $(a_1, \gamma_{th_1}) = (0.761, 2.8), (a_2, \gamma_{th_2}) = (0.191, 3)$ and $(a_3, \gamma_{th_3}) = (0.048, 3)$, and $(\sigma^2_{e,cee}, f_d) = (0.0014, 0)$. According to these test results, at low SNR values, the OP performance is the best for U_1, while in Rayleigh channel tests U_1 has the worst performance as in Fig. 15. This can be interpreted as the user with the longest channel, i.e., the most exposed to the channel, is the most affected by the channel hardness. On the other hand, for U_2 and U_3, the change in performance was not as dramatic as U_1. As another effect of the channel is the error floor levels of the curves tended towards 0 in the simulation results while they remained at 10^{-3} levels during the test.

In Fig. 17-(a), the results of JTRAS and TAS/MRC tests in the Nakagami channel are compared. It seems that the MRC technique in the relay and receivers provides performance enhancement for all users. Moreover, in tests, it was observed that the error floor level decreased to nearly 10^{-5} and even to 0 at higher SNR values. Accordingly, it can be interpreted that the instantaneous weakening in one of the antennas was able to be recovered by the other one. Fig. 17-(b) shows a comparison between TAS/MRC tests and simulations in Nakagami channel with $(m_1, m_2) = (5.26, 5.26)$. Although the simulation results are generally similar to test results, the test results cannot easily reach the $OP = 0$ value at SNR values above 10 dB as in the simulation. The reason of this is thought to be due to the synchronization errors and the fact that the channel is not known certainly. It is observed that the test performance has a stable and simulation-compatible behavior. However, it cannot be explained that the test system gives better results than simulation at low SNR values. Fig. 17-(c) demonstrates a comparison of TAS/MRC measurements in different channels. These curves show that the performance of all users improved with the improvement of the channel in both hops, as in the JTRAS tests. At the same time, we can observe the effect of the channel at the error floor level. In addition, the improvement in the channel affects the TAS/MRC system more than the JTRAS system. As a result, compared with Rayleigh tests, the Nakagami $m = 5.26$ channel increases TAS/MRC performance level much more than JTRAS.

VI. Conclusion

In this work, we examine the OP performance for the cooperative MIMO-NOMA system with the presence and absence of CEE&FD. The exact OP expressions are first derived jointly for the TAS/MRC and JTRAS schemes in Nakagami-*m* fading channels. Next, the lower bound and asymptotic expressions

of the OP are obtained in the practical and ideal cases, respectively. Finally, the theoretical analysis results are verified by the Monte Carlo simulation and SDR-based measurement. The results show that in the practical case, the OP reaches the EF in the high SNR region, thus the diversity order becomes zero while in the ideal case, non-zero diversity and array gains are achieved. Moreover, the OP performance enhances as the number of transmit and/or receive antennas increases and channel condition improves. However, the antenna configuration influences the users differently. In particular, the performance of U_1 improves better when the number of receive antennas of the second hop increases rather than when the numbers of the transmit and/or receive antennas of the first hop increase. On the other hand, the performance of U_2 and U_3 considerably enhances when the numbers of the transmit and/or receive antennas of the first hop increase. Furthermore, the OP performance gets worse as CEE or FD increases for any user, but with the increase of CEE and/or FD, all OP performances converge to the same OP. In addition, for all users, the optimal location of the relay becomes closer to the middle in the practical case (CEE&FD) as compared to that in the ideal case. Nevertheless, the optimal location of the relay becomes nearer to the BS when the number of the antennas of the second hop increases, whereas it becomes closer to the users when the channel condition of the first hop increases. Besides, for each user, there is an effective range of power allocation coefficient that achieves better OP performance as well optimum power allocation coefficient that achieves optimum OP. Also, the TAS/MRC scheme provides better performance than the JTRAS scheme as well as the AS schemes that based on majority offer better performance than AS schemes that based on A^3.

APPENDIX

A. Proof of Proposition 1

The error terms in (5) due to CEE&FD are considered as noise [36]. Then, the instantaneous $SINR_{j\to l}$ is generally expressed as

$$SINR_{j\to l} = \frac{\| r_{2,l}^S \|^2}{\| r_{2,l}^I \|^2 + \| r_{2,l}^E \|^2 + \| r_{2,l}^N \|^2}. \quad (25)$$

Using $G^2 = \frac{1}{P_1\rho_1^2\varphi_1 + P_1\sigma_{e_1}^2 + \sigma_1^2}$, Then, $\frac{\|r_{2,l}^S\|^2}{G^2} = \rho_1^2\rho_2^2\varphi_1\varphi_{2,l}P_1P_2a_j$, $\frac{\|r_{2,l}^I\|^2}{G^2} = \rho_1^2\rho_2^2\varphi_1\varphi_{2,l}P_1P_2\sum_{i=j+1}^{L}a_i$, $\frac{\|r_{2,l}^E\|^2}{G^2} = \sigma_{e_1}^2\sigma_{e_{2,l}}^2P_1P_2 + \rho_1^2\varphi_1\sigma_{e_{2,l}}^2P_1P_2 + \rho_2^2\varphi_{2,l}\sigma_{e_1}^2P_1P_2 + \rho_2^2\varphi_{2,l}P_2\sigma_1^2 + \sigma_{e_{2,l}}^2P_2\sigma_1^2$ and $\frac{\|r_{2,l}^N\|^2}{G^2} = \sigma_{2,l}^2(P_1\rho_1^2\varphi_1 + P_1\sigma_{e_1}^2 + \sigma_1^2)$. For mathematical tractability, $P_1 = P_2 = P$, $\sigma_1^2 = \sigma_{2,l}^2 = \sigma^2$ are assumed and $\gamma = \frac{P}{\sigma^2}$. Thus, $\frac{\|r_{2,l}^S\|^2}{\sigma^4G^2\rho_1^2\rho_2^2} = a_j\gamma^2\varphi_1\varphi_{2,l}$, $\frac{\|r_{2,l}^I\|^2}{\sigma^4G^2\rho_1^2\rho_2^2} = \gamma^2\varphi_1\varphi_{2,l}\sum_{i=j+1}^{L}a_i$ and $\frac{\|r_{2,l}^E\|^2+\|r_{2,l}^N\|^2}{\sigma^4G^2\rho_1^2\rho_2^2} = \gamma\varphi_1(\frac{\gamma\sigma_{e_{2,l}}^2+1}{\rho_2^2}) + \gamma\varphi_{2,l}(\frac{\gamma\sigma_{e_1}^2+1}{\rho_1^2}) + \frac{\gamma^2\sigma_{e_1}^2\sigma_{e_{2,l}}^2+\gamma\sigma_{e_{2,l}}^2+\gamma\sigma_{e_1}^2+1}{\rho_1^2\rho_2^2}$. Consequently, by substituting these expressions in (25), the expression of instantaneous $SINR_{j\to l}$ is achieved in (10).

B. Proof of Proposition 2

The OP_l in (17) is rewritten as

$$\begin{aligned} OP_l &= P_r\left(\varphi_1 < \frac{\theta_l^*(b_2\gamma\varphi_{2,l}+b_3)}{\gamma\varphi_{2,l}-b_1\gamma\theta_l^*}, \varphi_{2,l} > b_1\theta_l^*\right) \\ &= \underbrace{\int_0^{b_1\theta_l^*} f_{\varphi_{2,l}}(x)dx}_{I_1} \\ &\quad + \underbrace{\int_{b_1\theta_l^*}^{\infty} f_{\varphi_{2,l}}(x)F_{\varphi_1}\left(\frac{\theta_l^*(b_2\gamma x+b_3)}{\gamma x-b_1\gamma\theta_l^*}\right)dx}_{I_2}. \quad (26) \end{aligned}$$

Now, substituting (13) and (16) into I_2 in (26), I_2 can be rewritten as (27), shown at the bottom of the page.

Then, by change of variable $y = x - b_1\theta_l^*$, I_3 in (27) can be rewritten as

$$\begin{aligned} I_3 &= \int_0^{\infty}(y+b_1\theta_l^*)^{m_2\beta_{r_2}+s-1}e^{-\frac{m_2(t+1)(y+b_1\theta_l^*)}{\hat{\Omega}_2}} \\ &\quad\times\left(\frac{\gamma b_2(y+b_1\theta_l^*)+b_3}{y}\right)^k e^{-\frac{pm_1\theta_l^*(\gamma b_2(y+b_1\theta_l^*)+b_3)}{\gamma\Omega_1 y}}dy \\ &= e^{-\frac{m_2b_1\theta_l^*(t+1)}{\hat{\Omega}_2}}e^{-\frac{pm_1b_2\theta_l^*}{\Omega_1}} \\ &\quad\times\int_0^{\infty}\underbrace{(y+b_1\theta_l^*)^{m_2\beta_{r_2}+s-1}}_{J_1}\underbrace{(\gamma b_2y+\gamma b_1b_2\theta_l^*+b_3)^k}_{J_2} \\ &\quad\times e^{-\frac{m_2(t+1)y}{\hat{\Omega}_2}}y^{-k}e^{-\frac{pm_1\theta_l^*(\gamma b_1b_2\theta_l^*+b_3)}{\gamma\Omega_1 y}}dy. \quad (28) \end{aligned}$$

$$\begin{aligned} I_2 &= \underbrace{\int_{b_1\theta_l^*}^{\infty} f_{\varphi_{2,l}}(x)dx}_{1-I_1} \\ &\quad + \frac{(m_2/\hat{\Omega}_2)^{m_2\beta_{r_2}}}{\Gamma(m_2\beta_{r_2})}\sum_{q=1}^{3\beta_{t_2}}\sum_{t=0}^{q\beta-1}\sum_{s=0}^{t(m_2\beta_{r_2}-1)}\sum_{p=1}^{\beta_{t_1}}\sum_{k=0}^{p(m_1\beta_{r_1}-1)}\binom{q\beta-1}{t} \\ &\quad\times\binom{\beta_{t_1}}{p}(-1)^{t+p}q\beta\zeta_{(l,q)}\vartheta_s(t,m_2\beta_{r_2})\vartheta_k(p,m_1\beta_{r_1})\left(\frac{\theta_l^*}{\gamma}\right)^k \\ &\quad\underbrace{\int_{b_1\theta_l^*}^{\infty} x^{m_2\beta_{r_2}+s-1}e^{-\frac{m_2(t+1)x}{\hat{\Omega}_2}}\left(\frac{b_2\gamma x+b_3}{x-b_1\theta_l^*}\right)^k e^{-\frac{pm_1\theta_l^*(b_2\gamma x+b_3)}{\gamma\Omega_1(x-b_1\theta_l^*)}}dx}_{I_3}. \quad (27) \end{aligned}$$

By using the binomial theorem, J_1 and J_2 in (28) can be written, respectively as

$$J_1 = \sum_{k_1=0}^{m_2\beta_{r_2}+s-1} \binom{m_2\beta_{r_2}+s-1}{k_1} (b_1\theta_l^*)^{m_2\beta_{r_2}+s-1-k_1} y^{k_1}, \tag{29}$$

$$J_2 = \sum_{k_2=0}^{k} \binom{k}{k_2} (\gamma b_1 b_2 \theta_l^* + b_3)^{k-k_2} (\gamma b_2)^{k_2} y^{k_2}. \tag{30}$$

If (29) and (30) are substituted into (28), then I_3 can be stated as

$$\begin{aligned} I_3 = {} & e^{-\frac{m_2 b_1 \theta_l^*(t+1)}{\Omega_2}} e^{-\frac{pm_1 b_2 \theta_l^*}{\Omega_1}} \sum_{k_1=0}^{m_2\beta_{r_2}+s-1} \sum_{k_2=0}^{k} \\ & \times \binom{m_2\beta_{r_2}+s-1}{k_1} \binom{k}{k_2} (b_1\theta_l^*)^{m_2\beta_{r_2}+s-1-k_1} \\ & \times (\gamma b_1 b_2 \theta_l^* + b_3)^{k-k_2} (\gamma b_2)^{k_2} \\ & \times \underbrace{\int_0^\infty y^{k_1+k_2-k} e^{-\frac{m_2(t+1)y}{\Omega_2}} e^{-\frac{pm_1\theta_l^*(\gamma b_1 b_2 \theta_l^* + b_3)}{\gamma \Omega_1 y}} dy}_{I_4} \end{aligned} \tag{31}$$

By the help [37], eq.(3.471.9)], I_4 in (31) is simply written in terms of $K_u(\cdot)$, $I_4 = 2(\frac{c_1}{c_2})^{\frac{k_1+k_2-k+1}{2}} K_{k_1+k_2-k+1}(2\sqrt{c_1 c_2})$. Then, I_3 in (31) can be expressed as

$$\begin{aligned} I_3 = {} & e^{-\frac{m_2 b_1 \theta_l^*(t+1)}{\Omega_2}} e^{-\frac{pm_1 b_2 \theta_l^*}{\Omega_1}} \sum_{k_1=0}^{m_2\beta_{r_2}+s-1} \sum_{k_2=0}^{k} \\ & \times \binom{m_2\beta_{r_2}+s-1}{k_1} \binom{k}{k_2} (b_1\theta_l^*)^{m_2\beta_{r_2}+s-1-k_1} \\ & \times (\gamma b_1 b_2 \theta_l^* + b_3)^{k-k_2} (\gamma b_2)^{k_2} \times 2(\frac{c_1}{c_2})^{\frac{k_1+k_2-k+1}{2}} \\ & \times K_{k_1+k_2-k+1}(2\sqrt{c_1 c_2}). \end{aligned} \tag{32}$$

Therefore, by substituting (32) and (27) into (26), the exact OP_l is obtained as in (18).

REFERENCES

[1] L. Dai, B. Wang, Y. Yuan, S. Han, and Z. Wang, "Non-orthogonal multiple access for 5G: Solutions, challenges, opportunities, and future research trends," *IEEE Commun. Mag.*, vol. 53, no. 9, pp. 74–81, Sep. 2015.

[2] M. Aldababsa *et al.*, "A tutorial on non-orthogonal multiple access (NOMA) for 5G and beyond," *J. Wireless Commun. Mobile Comput.*, vol. 83, pp. 83–98, Jun. 2018.

[3] S. M. R. Islam, N. Avazov, O. A. Dobre, and K.-S. Kwak, "Power-domain non-orthogonal multiple access (NOMA) in 5G systems: Potentials and challenges," *IEEE Commun. Surveys Tuts.*, vol. 19, no. 2, pp. 721–742, 2nd Quart., 2017.

[4] E. Telatar, "Capacity of multi-antenna Gaussian channels," *Eur. Trans. Telecommun.*, vol. 10, no. 6, pp. 585–596, Nov. 1999.

[5] A. F. Molisch and M. Z. Win, "MIMO systems with antenna selection," *IEEE Commun. Mag.*, vol. 5, no. 1, pp. 46–56, Mar. 2004.

[6] J. N. Laneman and G. W. Wornell, "Energy-efficient antenna sharing and relaying for wireless networks," in *Proc. IEEE WCNC*, vol. 1, Chicago, IL, USA, Sep. 2000, pp. 7–12.

[7] Z. Zhao and W. Chen, "An adaptive switching method for sum rate maximization in downlink MISO-NOMA systems," in *Proc. IEEE Global Commun. Conf.*, Singapore, Dec. 2017, pp. 1–6.

[8] M. Toka and O. Kucur, "Non-orthogonal multiple access with Alamouti space–time block coding," *IEEE Commun. Lett.*, vol. 22, no. 9, pp. 1954–1957, Sep. 2018.

[9] M. Li, H. Yuan, X. Yue, S. Muhaidat, C. Maple, and M. Dianati, "Secrecy outage analysis for Alamouti space–time block coded non-orthogonal multiple access," *IEEE Commun. Lett.*, vol. 24, no. 7, pp. 1405–1409, Jul. 2020.

[10] L. Guowei and S. Sunqing, "Antenna selection for non-orthogonal multiple access with space time block codes," in *Proc. IEEE 8th Int. Conf. Inf., Commun. Netw. (ICICN)*, Xian, China, Aug. 2020, pp. 141–145.

[11] M. Toka and O. Kucur, "Performance analysis of OSTBC-NOMA system in the presence of practical impairments," *IEEE Trans. Veh. Technol.*, vol. 69, no. 9, pp. 9697–9706, Sep. 2020.

[12] A. P. Shrestha, T. Han, Z. Bai, J. M. Kim, and K. S. Kwak, "Performance of transmit antenna selection in non-orthogonal multiple access for 5G systems," in *Proc. 8th Int. Conf. Ubiquitous Future Netw. (ICUFN)*, Vienna, NSE, Austria, Jul. 2016, pp. 1031–1034.

[13] S. Ustunbas and U. Aygolu, "Transmit antenna selection based on sum rate and fairness for downlink NOMA," in *Proc. Telecommun. Forum*, Belgrade, Serbia, 2017, pp. 1–4.

[14] H. Lei *et al.*, "On secure NOMA systems with transmit antenna selection schemes," *IEEE Access*, vol. 5, pp. 17450–17464, 2017.

[15] D.-D. Tran, H.-V. Tran, D.-B. Ha, and G. Kaddoum, "Secure transmit antenna selection protocol for MIMO NOMA networks over Nakagami-m channels," *IEEE Syst. J.*, vol. 14, no. 1, pp. 253–264, Mar. 2020.

[16] H. Lei *et al.*, "Secrecy outage of max–min TAS scheme in MIMO-NOMA systems," *IEEE Trans. Veh. Technol.*, vol. 67, no. 8, pp. 6981–6990, Aug. 2018.

[17] M. Aldababsa and O. Kucur, "Outage performance of NOMA with majority based TAS/MRC scheme in Rayleigh fading channels," in *Proc. 27th Signal Process. Commun. Appl. Conf. (SIU)*, Sivas, Turkey, Apr. 2019, pp. 1–4.

[18] M. Aldababsa and O. Kucur, "Majority based antenna selection schemes in downlink NOMA network with channel estimation errors and feedback delay," *IET Commun.*, vol. 14, no. 17, pp. 2931–2943, Oct. 2020.

[19] M. Aldababsa and O. Kucur, "BER performance of NOMA network with majority based JTRAS scheme in practical impairments," *AEU-Int. J. Electron. Commun.*, vol. 129, Feb. 2021, Art. no. 153523.

[20] Y. Yu, H. Chen, Y. Li, Z. Ding, L. Song, and B. Vucetic, "Antenna selection for MIMO nonorthogonal multiple access systems," *IEEE Trans. Veh. Technol.*, vol. 67, no. 4, pp. 3158–3171, Apr. 2018.

[21] Q. Li, J. Ge, Q. Wang, and Q. Bu, "Joint antenna selection for MIMO-NOMA networks over Nakagami-m fading channels," in *Proc. IEEE/CIC Int. Conf. Commun. China (ICCC)*, Qingdao, China, Oct. 2017, pp. 1–6.

[22] Y. Yu, H. Chen, Y. Li, Z. Ding, and L. Zhuo, "Antenna selection in MIMO cognitive radio-inspired NOMA systems," *IEEE Commun. Lett.*, vol. 21, no. 12, pp. 2658–2661, Dec. 2017.

[23] M. Aldababsa and O. Kucur, "Cooperative NOMA with antenna selection schemes," in *Proc. 27th Signal Process. Commun. Appl. Conf. (SIU)*, Sivas, Turkey, Apr. 2019, pp. 1–4.

[24] J. Men and J. Ge, "Non-orthogonal multiple access for multiple-antenna relaying networks," *IEEE Commun. Lett.*, vol. 19, no. 10, pp. 1686–1689, Oct. 2015.

[25] M. Aldababsa and O. Kucur, "Outage performance of NOMA with TAS/MRC in dual hop AF relaying networks," in *Proc. Adv. Wireless Opt. Commun.*, Riga, Latvia, 2017, pp. 137–141.

[26] W. Han, J. Ge, and J. Men, "Performance analysis for NOMA energy harvesting relaying networks with transmit antenna selection and maximal-ratio combining over Nakagami-m fading," *IET Commun.*, vol. 10, no. 18, pp. 2687–2693, Dec. 2016.

[27] Q. Wang, J. Ge, Q. Li, and Q. Bu, "Performance analysis of NOMA for multiple-antenna relaying networks with energy harvesting over Nakagami-m fading channels," in *Proc. IEEE/CIC Int. Conf. Commun. China (ICCC)*, Qingdao, China, Oct. 2017, pp. 1–5.

[28] Y. Zhang, J. Ge, and E. Serpedin, "Performance analysis of nonorthogonal multiple access for downlink networks with antenna selection over Nakagami-m fading channels," *IEEE Trans. Veh. Technol.*, vol. 66, no. 11, pp. 10590–10594, Nov. 2017.

[29] M. Aldababsa and O. Kucur, "Outage and ergodic sum-rate performance of cooperative MIMO-NOMA with imperfect CSI and SIC," *Int. J. Commun. Syst.*, vol. 33, no. 11, p. e4405, Jul. 2020.

[30] M. Aldababsa and O. Kucur, "Performance of cooperative multiple-input multiple-output NOMA in Nakagami-m fading channels with channel estimation errors," *IET Commun.*, vol. 14, no. 2, pp. 274–281, Jan. 2020.

[31] A. Yélmaz and O. Kucur, "Unified analysis of transmit, receive and hybrid diversity techniques over generalized-kchannels," *Wireless Commun. Mobile Comput.*, vol. 16, no. 13, pp. 1798–1808, Sep. 2016.
[32] T. R. Ramya and S. Bhashyam, "Using delayed feedback for antenna selection in MIMO systems," *IEEE Trans. Wireless Commun.*, vol. 8, no. 12, pp. 6059–6067, Dec. 2009.
[33] M. Médard, "The effect upon channel capacity in wireless communications of perfect and imperfect knowledge of the channel," *IEEE Trans. Inf. Theory*, vol. 46, no. 3, pp. 933–946, May 2000.
[34] N.-S. Kim and Y. H. Lee, "Effect of channel estimation errors and feedback delay on the performance of closed-loop transmit diversity system," in *Proc. Workshop Signal Process. Adv. Wireless Commun.*, Rome, Italy, 2003, pp. 542–545.
[35] W. C. Jakes, *Microwave Mobile Communication*. New York, NY, USA: Wiley, 1974.
[36] Y. Chen and C. Tellambura, "Performance analysis of maximum ratio transmission with imperfect channel estimation," *IEEE Commun. Lett.*, vol. 9, no. 4, pp. 322–324, Apr. 2005.
[37] IS. Gradshteyn and IM. Ryzhik, *Table of Integrals, Series, and Products*, 7th ed. San Diego, CA, USA: Academic, 2007.
[38] P. A. Anghel and M. Kaveh, "Exact symbol error probability of a cooperative network in a Rayleigh-fading environment," *IEEE Trans. Wireless Commun.*, vol. 3, no. 5, pp. 1416–1421, Sep. 2004.
[39] Z. Wang and G. B. Giannakis, "A simple and general parameterization quantifying performance in fading channels," *IEEE Trans. Commun.*, vol. 51, no. 8, pp. 1389–1398, Aug. 2003.
[40] K. B. Oldham, *An Atlas Functions with Equator, Atlas Function Calculator*, 2nd ed. Berlin, Germany: Springer, 2008.

Mahmoud Aldababsa received the B.Sc. degree in electrical engineering from An-Najah National University, Palestine, in 2010, the M.Sc. degree in electronics and communication engineering from Al-Quds University, Palestine, in 2013, and the Ph.D. degree in electronics engineering from Gebze Technical University, Turkey. He was a Research Assistant at Al-Quds University from 2010 to 2013. He was a Post-Doctoral Researcher at the Communications Research and Innovation Laboratory (CoreLab), Koç University, Turkey. Currently, he is an Assistant Professor of electrical and electronics engineering at Istanbul Gelisim University, Turkey. His current research interests include non-orthogonal multiple access and reconfigurable intelligent surface in beyond 5G and 6G wireless systems.

Eray Güven received the B.S. degree in electronics and communication engineering from Istanbul Technical University, Istanbul, Turkey, in 2021, where he is currently pursuing the master's degree in telecommunication engineering.

M. Akif Durmaz received the B.Sc. degree in electronics and telecommunication engineering and the M.Sc. degree in satellite communication and remote sensing from Istanbul Technical University (ITU), Istanbul, Turkey, in 2017 and 2021, respectively. He is currently working with Turkcell Technology 5G Research and Development Team, Istanbul. His research interests are 5G and beyond technologies and SDR applications.

Caner Göztepe received the B.Sc. and M.Sc. degrees in telecommunication engineering from Istanbul Technical University (ITU), Turkey, in 2017 and 2019, respectively, where he is currently pursuing the Ph.D. degree. His research interests are 5G+, physical layer security, and SDR applications beyond 5G physical layer schemes.

Güneş Karabulut Kurt (Senior Member, IEEE) received the B.S. degree (Hons.) in electronics and electrical engineering from Boğaziçi University, Istanbul, Turkey, in 2000, and the M.A.Sc. and Ph.D. degrees in electrical engineering from the University of Ottawa, ON, Canada, in 2002 and 2006, respectively. From 2000 to 2005, she was a Research Assistant with the CASP Group, University of Ottawa. From 2005 to 2006, she was with TenXc Wireless, Canada. From 2006 to 2008, she was with Edgewater Computer Systems Inc., Canada. From 2008 to 2010, she was with Turkcell Research and Development Applied Research and Technology, Istanbul. From 2010 to 2021, she was with Istanbul Technical University. She is currently an Associate Professor of electrical engineering at Polytechnique Montréal, Montréal, QC, Canada. She is also an Adjunct Research Professor at Carleton University. She is a Marie Curie Fellow and has received the Turkish Academy of Sciences Outstanding Young Scientist (TÜBA-GEBIP) Award in 2019. She is serving as a member for the IEEE WCNC Steering Board and an Associate Technical Editor (ATE) for the *IEEE Communications Magazine*.

Oğuz Kucur received the B.S. degree in electronics and telecommunication engineering from Istanbul Technical University, Istanbul, Turkey, in 1988, and the M.S. and Ph.D. degrees in electrical and computer engineering from the Illinois Institute of Technology (IIT), Chicago, USA, in 1992 and 1998, respectively. From 1996 to 1998, he was a Teaching Assistant at IIT. He was an Assistant Professor with the Department of Electrical Engineering, South Dakota State University, from 1998 to 1999. Since 1999, he has been with the Department of Electronics Engineering, Gebze Technical University, Turkey, where he is currently a Professor. His research interests are fading channels and diversity techniques, multi-user communications, MIMO, and cooperative communications.